

Review

Hemocompatibility of Carbon Nanostructures

Mariangela Fedel 

Center for Health & Bioresources, Biomedical Systems, AIT Austrian Institute of Technology GmbH,
2700 Wiener Neustadt, Austria; mariangela.fedel@ait.ac.at

Received: 31 January 2020; Accepted: 28 February 2020; Published: 5 March 2020



Abstract: Carbon nanostructures (CNs), such as carbon nanotubes, fullerenes, carbon dots, nanodiamonds as well as graphene and its derivatives present a tremendous potential for various biomedical applications, ranging from sensing to drug delivery and gene therapy, biomedical imaging and tissue engineering. Since most of these applications encompass blood contact or intravenous injection, hemocompatibility is a critical aspect that must be carefully considered to take advantage of CN exceptional characteristics while allowing their safe use. This review discusses the hemocompatibility of different classes of CNs with the purpose of providing biomaterial scientists with a comprehensive vision of the interactions between CNs and blood components. The various complex mechanisms involved in blood compatibility, including coagulation, hemolysis, as well as the activation of complement, platelets, and leukocytes will be considered. Special attention will be paid to the role of CN size, structure, and surface properties in the formation of the protein corona and in the processes that drive blood response. The aim of this review is to emphasize the importance of hemocompatibility for CNs intended for biomedical applications and to provide some valuable insights for the development of new generation particles with improved performance and safety in the physiological environment.

Keywords: nanodiamonds; fullerenes; carbon dots; carbon nanotubes; graphene; plasma proteins; blood coagulation; complement activation; platelets; hemolysis

1. Introduction

Due to its ability to assume different hybridization states, including sp^2 and sp^3 hybridization, carbon can form different allotropes (e.g., graphite, diamond, and fullerene-like structures) which exhibit peculiar chemical and physical characteristics derived from their specific structure. A range of carbon nanostructures (CNs) have recently raised the interest of material scientists due to the extraordinary characteristics related to their nanoscale size. Among carbon nanostructures, we can count 0-D systems such as nanodiamonds (NDs), fullerenes (CFs) and carbon dots (CDs), 1-D carbon nanotubes (CNTs) and nanofibers, as well as 2-D graphene-based nanostructures (GBNs) (Figure 1). Due to their outstanding physical, chemical, mechanical, thermal, electrical and optical properties [1], CNs are extremely attractive for a wide range of applications in electronics, optoelectronics, sensing, mechanics, construction, automotive, and aerospace fields [2–5].

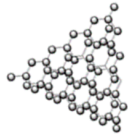
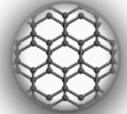
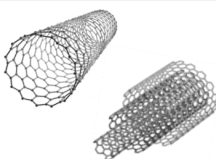
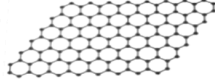
CARBON NANOSTRUCTURES				
0-D			1-D	2-D
				
Nanodiamonds (NDs)	Carbon Fullerenes (CFs)	Carbon Dots (CDs)	Carbon Nanotubes (CNTs)	Graphene

Figure 1. Main forms of carbon nanostructures (not to scale).

In the biomedical field CNs have been proposed for a number of theragnostic applications [6,7], including biosensing [8], imaging [9,10], hyperthermal cancer therapy, stem cell therapy, tissue engineering [11–13], drug and gene delivery. Due to their small size, high specific surface area, and easy surface functionalization, NDs, CDs, CFs, CNTs, and GBNs have shown promising results as transporting systems for the administration of proteins, nucleic acids, and pharmaceutical compounds [14–17], and have demonstrated to successfully increase the efficacy of distribution and cell uptake of poorly permeating molecules. Thanks to their surface chemistry, most CNs can be easily conjugated with various functional groups and chemical moieties in an attempt to improve some features that are critical in the biological environment (e.g., colloidal dispersibility and stability), to address the desired biological response or to reach specific target organs. Various active molecules, including chemotherapeutics, antiretroviral, antibacterial, and anti-inflammatory compounds [18–20], have been conjugated to CNs with high drug loading efficiency.

CNs are undoubtedly a powerful platform for developing forefront theragnostic tools. However, the growing interest in using CNs in the biomedical field has raised significant concerns about their biocompatibility, clearly pointing out that the effects of the nanostructures on the biological environment must be carefully assessed in order to take full advantage of their unique characteristics and to define their safe use. The cytotoxicity and immunological response of different types of CNs have been thoroughly investigated both *in vitro* and *in vivo*, disclosing a quite complex landscape [21–24]. Experimental studies have shown that cell response depends on several factors, such as CN physicochemical properties and geometrical structure, surface functionalization, size distribution, presence of impurities, wettability and dispersibility in aqueous media, as well as on the culture medium and target cell type [25–32]. The literature in this field is copious and detailed information can be found in some recent reviews dealing with the biocompatibility, biodistribution, and biodegradation of different types of CNs [33–36]. Much less effort has been dedicated to the study of CN hemocompatibility, although most biomedical applications (e.g., drug delivery, imaging, etc.) require direct intravenous administration or involve blood contact as a consequence of local administration or translocation to the blood stream following inhalation or ingestion. Hemocompatibility represents a critical issue towards the safe *in vivo* utilization of nanomaterials for diagnostic and therapeutic purposes and can significantly contribute to define their success or failure in the biomedical field. Therefore, analyzing the interactions of CNs with blood is of paramount concern for determining their fate in the physiological environment and for identifying potential adverse effects.

After a brief general overview of the complex mechanisms that can take part in the blood-material interactions and of the specific issues related to nanosized objects, this review will provide a comprehensive revision of the main hemocompatibility studies conducted by experimental and theoretical modeling analyses on different classes of CNs, including nanodiamonds, fullerenes, carbon dots, carbon nanotubes, and graphene and its derivatives. We will individually examine the characteristics of different types of carbon-based nanostructures and discuss their effects on the

various blood components, including plasma proteins, complement and coagulation factors, platelets (PLTs), and red blood cells (RBCs). The parameters affecting CN hemocompatibility will be discussed, in an attempt to identify common features and recurrent pathways dictating the interaction rules. Potentialities and weaknesses of CN use in specific blood-contacting applications will be critically examined, and the strategies proposed in the literature for improving the hemocompatibility of the different classes of CNs for biomedical applications will be described.

2. Hemocompatibility of Biomaterials—Short Overview

Blood is a very complex biological tissue composed of a liquid (plasma) and a solid phase (blood cells), where different biochemical mechanisms and reactions take place in order to maintain the homeostasis of the physiological system. The blood cellular component is formed by red blood cells (erythrocytes), white blood cells (monocytes, lymphocytes, neutrophils, eosinophils, basophils, and macrophages), and platelets, while plasma contains, in addition to electrolytes and other biomolecules, hundreds of proteins with different concentrations, properties and functions. “When blood is touched”, to use the words of Leo Vroman [37], one of the first and most well-known hematologists to study the behavior of blood following contact with natural and artificial surfaces, a series of complex and interconnected processes can be activated. These include protein adsorption, platelet adhesion, activation and aggregation, activation of the coagulation cascade and of the complement system, as well as hemolysis.

Protein adsorption is the first event taking place when biomaterials are exposed to a biological environment. Within a few seconds after blood–material contact, the surface is covered with a layer of proteins, whose composition, relative concentration, conformation, and orientation guide the consequent host response and contribute to determine the fate of the material [38]. Protein adsorption on biomaterials from multicomponent solutions, such as plasma, is a dynamic process that includes the transport of proteins to the exposed surface and a first reversible binding followed by exchange phenomena among different species [39,40]. Nearly 300 proteins with different molecular weight, charge, structure, and concentration have been detected in plasma to date [41]. Among these, about a dozen proteins (“the big twelve”) [42] are considered to dominate plasma protein adsorption, including human serum albumin (HSA), immunoglobulins (IgG, IgA, IgM), C3 complement component, fibrinogen (Fng), haptoglobin, α 1-antitrypsin, α 2-macroglobulin, as well as low- and high-density lipoproteins.

Both the physicochemical properties of the material (e.g., chemical composition and functionalization, surface roughness, wettability, water sorption, etc.) [43] and the characteristics of the proteins in solution (e.g., amino-acid composition, size, structure, presence of polar or charged domains, isoelectric point, etc.) contribute to control the adsorption process and to define the type, amount, and conformation of the bound molecules. The adsorbed protein layer plays then a pivotal role in guiding the overall response of biomaterials in terms of hemocompatibility. Platelet and leukocyte adhesion/activation phenomena as well as activation of the complement system and of the intrinsic coagulation pathway may result from a specific protein adsorption. For example, it is well known that adsorbed adhesive plasma proteins such as fibrinogen, von Willebrand Factor, and fibronectin are responsible for platelet adhesion and that activated platelets can, in turn, act as pro-adhesive mediators for leukocytes [44].

When proteins encounter significant modifications in their three-dimensional structure upon adsorption (e.g., molecular spreading or unfolding) their original function can be altered, and subsequent biological reactions may be induced [45]. This may involve the exposition of otherwise masked specific functional groups or biologically active moieties to the surrounding environment. For instance, it was shown that, while soluble Fng does not bind resting platelets, the exposure of the carboxyl terminus of the Fng γ -chain induced during adsorption on pro-thrombotic surfaces allows the binding to platelet GPIIb/IIIa receptors and leads to Fng-mediated platelet adhesion [46].

Platelet adhesion can be followed by a cascade of biochemical signals, that rapidly initiate platelet activation, including change of shape, release of PLT granules content (e.g., Platelet Factor-4, Fng, ADP, serotonin, Ca^{++} , etc.), formation of small amounts of thrombin and generation of thromboxane A_2 .

The released substances, in particular Fng, stimulate platelet aggregation leading to the formation of the so called “white” thrombus.

In parallel with platelet adhesion and activation, the intrinsic pathway of coagulation can be initiated by contact activation. The activation of surface-bound contact phase proteins (e.g., FXII) promotes a series of Ca^{++} -dependent reactions and culminates with the conversion of prothrombin (FII) to thrombin [47]. Thrombin, in turn, acts on fibrinogen, producing small fibrinopeptides, which polymerize to form an organized fibrin mesh stabilized by FXIII, which can incorporate red blood cells to form the “red” blood clot. At least 12 factors, mainly belonging to the serine protease family, are involved in the coagulation process.

Complement activation is another detrimental effect that may take place when materials are exposed to blood. As part of the innate immune system, complement is composed of small plasma circulating proteins and factors that can induce a series of inflammatory responses to help fighting foreign cells and organisms. Material-induced complement activation can occur via the classical or alternative pathway. An exhaustive description of the complex mechanisms involved in complement activation on artificial surfaces and of its contribution in adverse reactions, including leukocyte activation and inflammatory reaction, can be found elsewhere [47–50]. In brief, both the classical and alternative pathways contribute to the formation of C3 convertase complexes (C4bC2a and C3bBb, respectively) that cleave the C3 complement component into C3a and C3b. The anaphylatoxin C3a induces pro-inflammatory effects, including neutrophil and macrophage chemoattraction, while surface-immobilized C3b recruits and activates leukocytes and binds to pathogens inducing their phagocytosis. C3b also takes part in the formation of the C3 and C5 convertase, which generates the pro-inflammatory anaphylatoxin C5a [51] and the fragment C5b, which may induce the formation of the terminal complement complexes (TCC or sC5b-9). Surface adsorbed plasma proteins play a key role in the activation of the complement system, as specific conformational changes in the molecular structure of adsorbed proteins can expose varying number of acceptor sites to C3 fragments [52]. Moreover, it was shown that conformational changes in the C3 opsonins adsorbed to a material surface can generate C3 convertases, which, in turn, can trigger further activation and amplification of the alternative complement pathway [53].

All the above-mentioned processes that can occur at the blood-material interface (Figure 2) are closely interconnected [54]. For example, the initiating factor of the intrinsic coagulation cascade, FXIIa, contributes to complement activation, while the activity of the complement system can contribute to the amplification of the coagulation cascade [55]. In addition, platelet phospholipidic membrane represents an essential substrate for the formation of active complexes during the coagulation process and thrombin generation activates platelets, which then catalyze the production of more thrombin.

The exposition of biomaterials to blood may also cause hemolysis, which is the loss of RBC membrane integrity resulting in the release of intracellular hemoglobin (Hb) into plasma. The modification and lysis of erythrocytes can induce anemia, alteration of kidney function and other pathological conditions.

Standard practices for testing the interactions of medical devices with blood are specified in the reference standard ISO 10993-4.

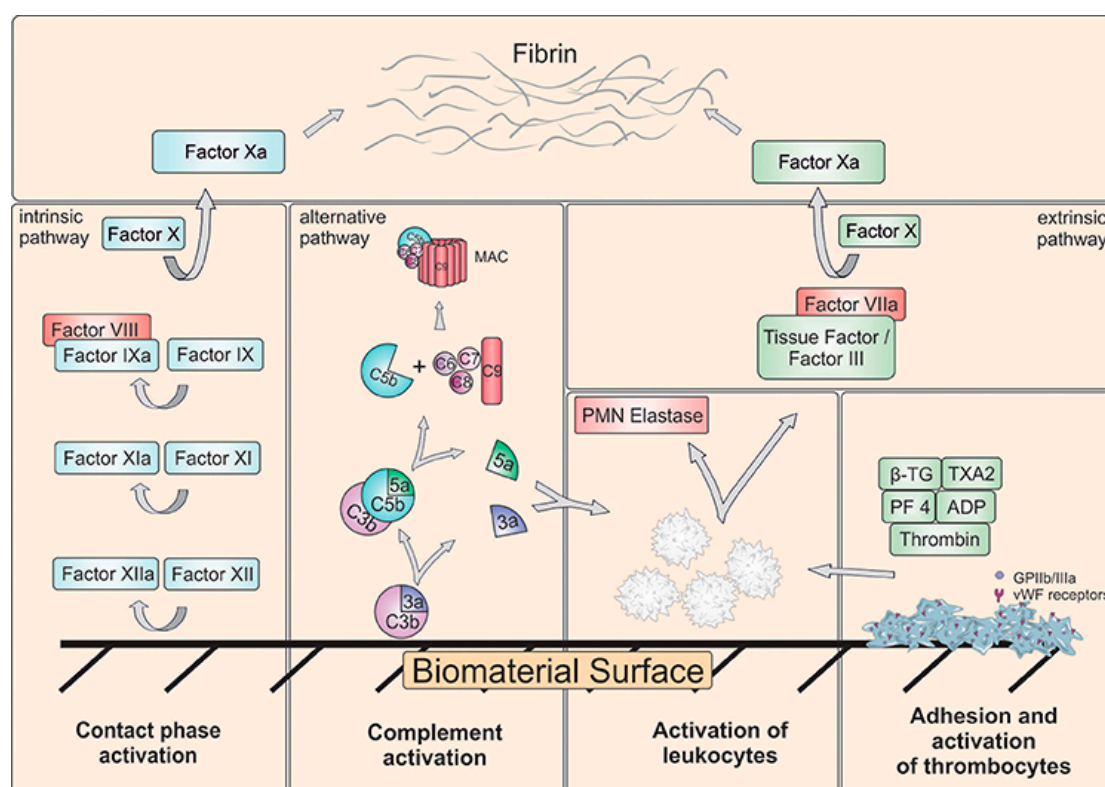


Figure 2. Schematic representation of the main biological processes that can occur at the blood-biomaterial surface. Reproduced with permission from [54].

Blood–Material Interactions at the Nanoscale

As any biomaterial involving blood contact at some level, nanostructures intended for biomedical applications require an in-deep investigation to assess the absence of adverse effects in the blood environment. However, while the interactions of blood components with macroscopic biomaterials are quite well known at the present time, the interactions with nanometric-sized objects have not been completely elucidated yet. Blood-NP interactions involve, in fact, original aspects, mainly related to the NP extremely high surface-to-volume ratio and surface energy, and exhibit a superior degree of methodological complexity due to borderline experimental conditions and sophisticated equipment required for the analysis.

At the nanometric level materials can assume unusual properties and their behavior can differ significantly from that of their macroscopic counterparts. In addition to surface chemistry, roughness, crystallinity, and wettability, in the case of nano-sized objects some other physicochemical characteristics contribute to define their interactions with the biological environment, including nanoparticle shape, size and surface area, curvature radius, surface energy, charge, presence of functional groups, hydration, and particle dispersion/aggregation [56]. All these characteristics, as well as some properties of the suspending media as ionic strength, pH, temperature and presence of biomolecules (e.g., proteins), have a significant role in guiding the hemocompatibility of the nanostructures. In particular, the protein adsorption process is extremely sensitive to the nanomaterial physicochemical properties.

Protein Corona

Once injected in a biological fluid, such as blood plasma, nanoparticles (NPs) are rapidly coated with a layer of proteins forming the so-called “protein corona” [57,58] in a dynamic process which does not reach the thermodynamic equilibrium [59]. The corona is typically composed of a “hard” portion formed by a thin inner layer of more closely bound proteins, and a “soft” outer layer with less tightly bound and fast exchanging proteins. Hydrophobic interactions, electrostatic interactions,

van der Waals interactions, hydrogen bonds, and π - π stacking can contribute in various degree to NP-protein interaction depending on the nature of both nanomaterials and protein media. The protein corona represents the new and dynamic NP interface with the external environment. Experimental studies investigating the nature and composition of the protein corona presented disparate outcomes, both because of the variety of NP and because of the different analytical methods used. A set of 125 plasma proteins has been found to associate with nanomaterials [60], and among these albumin, immunoglobulins, apolipoprotein A-I, and complement components have been frequently found in the nanomaterial corona [61]. If the proteins forming the corona undergo conformational changes with respect to their native structure, their functionality may be impaired, and their regular biological activity may be altered, causing abnormal interactions with other blood components [62]. Thus, the global NP-protein system is responsible for potential adverse events in the cardiovascular system, including thrombosis, complement and leukocyte activation, and hemolysis. Opsonization by complement components and immunoglobulins can, for example, cause the activation of the immune system and receptor-mediated phagocytosis, influencing the rapidity of clearance from the blood stream and/or the biodistribution in different target organs. The blood protein corona has also effects on NP dispersion/aggregation, as well as on circulation time, biodistribution and targeting efficiency of nanomedicines [63], and in some cases was hypothesized to contribute protecting RBC membrane from lysis [64]. Despite considerable challenges due to the shortage of adequate techniques and protocols for the analysis of the extremely complex nano(protein)-to-nano(material) interaction phenomena, a better knowledge of NP-protein interactions, including molecular mechanisms involved and potential induced biological effects is the first step towards a full understanding of NPs hemocompatibility [65,66].

3. Carbon Nanodiamonds

Carbon nanodiamonds are nanosized particles with the allotropic form of diamond. They can be synthesized by different techniques as detonation, chemical vapor deposition, laser ablation, ultrasound cavitation, and high energy ball milling of microdiamonds produced using high pressure and high temperature [67]. In particular, detonation is currently a popular and inexpensive technique, which can lead to single-crystalline diamond nanoparticles with an average size of ca. 4–5 nm after the post-processing procedure based on purification, de-aggregation and fractionation [68]. Surface modification (e.g., with amine, carboxyl, hydroxyl, ether or ester terminations, as well as with biomolecules) and doping (e.g., with transition metals, Si, N) are two strategies adopted to control and improve the properties of NDs for biomedical applications [7,69]. Exceptional optical and mechanical properties, including high hardness, low coefficient of friction, and wear resistance, as well as high chemical and thermal resistance, make ND an excellent candidate for *in vivo* imaging [70], selective targeting [15], gene and drug delivery (also for water-insoluble therapeutics) [71], for developing nanorobots [67], or for use as filler in tissue engineering scaffolds [72–74].

Diamond nanoparticles exhibited quite good cytocompatibility, with a low toxicity profile, as proved by *in vitro* studies with different cell types including human osteosarcoma (MG-63) [75], liver (HepG2 and Hep3B), kidney (Caki-1 and Hek-293), intestine (HT29), and lung (A549) cell lines [76,77].

Protein adsorption on NDs seems to be prevalently driven by hydrophobic interactions, or by electrostatic forces in the case of charged NDs. In particular, negatively-charged NDs presented a significantly higher binding affinity for proteins (myoglobin, bovine serum albumin (BSA), and insulin) with respect to positively-charged NDs [78]. Aramesh and colleagues analyzed the adsorption kinetics and structural characteristics of BSA and lysozyme as model proteins on hydrogen-terminated and oxygen-terminated charged nanodiamond particles [79]. The adsorption process on charged NDs was mainly driven by electrostatic interactions, generated by local pH changes surrounding the charged nanoparticles, which, in turn, caused further changes in the local protein charge, hydration layer, and overall affinity for the ND surface. According to the electrostatic model proposed, the small lysozyme proteins underwent strong conformational modifications and dehydration during a multistage adsorption process, while larger BSA molecules presented only minor structural changes [79].

Strong interaction of BSA with NDs and dominance of hydrophobic forces in the adsorption process were reported in the work of Wang et al. [80]. By means of spectroscopic studies the authors showed that NDs induced some conformational changes in the secondary structure of albumin, even though protein unfolding was not significant and most of the structural features of BSA were preserved in the ND-BSA complex [80].

Carboxylated NDs incubated with human blood plasma were found to induce protein adsorption without affecting the secondary structure. This seems to have a positive effect on hemocompatibility, since COOH-NDs (5 nm and 100 nm diameter) at concentrations in the range of 10 to 500 $\mu\text{g/mL}$ did not cause any significant modifications in the intrinsic pathway of coagulation as measured by activated partial thromboplastin times (aPTT) in line with those of normal human plasma [81]. Colloidal solutions of carboxylated detonation NDs (4–10 nm size) at 1–5 $\mu\text{g/mL}$ induced several concentration-dependent modifications on blood platelets *in vitro*, including aggregation, morphological alterations, increase of free intracellular Ca^{2+} level, and attenuation of viability [82]. In the same experimental study, using a murine model of pulmonary thromboembolism, Kumari et al. showed that NDs may elicit strong thromboembolic effects *in vivo*. However, the extremely drastic effects of NDs on blood compatibility presented in this research do not find validation in other recent works. A completely different behavior was shown by Li and colleagues, who examined the blood compatibility of nano-sized diamond crystallites (10% ca. -COOH surface groups) synthesized by high-pressure/high-temperature and purified by air oxidation and strong oxidative acid treatment [83]. Different samples ranging from 35 nm to 500 nm in diameter were tested in the study at concentrations up to 400 $\mu\text{g/mL}$, showing negligible hemolytic and thrombogenic effects irrespectively from NDs size and colloidal concentration (Figure 3). In addition, the presence of ND-induced inflammation was excluded by *in vivo* tests on adult mice, so that these oxidized type NDs was proposed for heparin delivery [83].

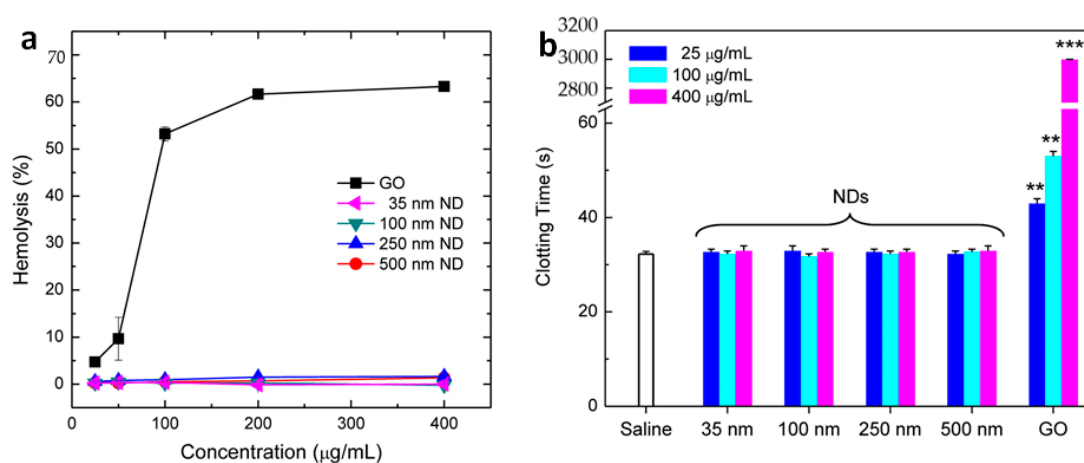


Figure 3. (a) Hemolysis percentages measured by exposition of RBCs to ND (35, 100, 250, and 500 nm in diameter) and graphene oxide (GO) samples at the concentration range of 25–400 $\mu\text{g/mL}$. Reproduced with permission from [83]. (b) Activated partial thromboplastin time (aPTT) assays of GOs and oxidized NDs of different size using human serum. ** $p < 0.01$ and *** $p < 0.001$ Reproduced with permission from [83]. NDs showed significantly lower hemolysis respect to GO and values comparable to saline negative control for the aPTT.

Good compatibility of detonated NDs with RBCs was reported by Wasowicz et al., who demonstrated the absence of any hemolytic activity induced by either commercial unmodified, oxygenated (hydrophilic) or hydrogenated (hydrophobic) NDs [84]. Drastic effects of NDs on white and red blood cells, with significant modification of active oxygen generation kinetics and hemolysis, have been reported in one of the first *in vitro* experiments considering the interaction of NDs with human blood components [85]. Conversely, more recent studies have revealed that the exposure of human RBCs to NDs (5 and 100 nm) may affect the deformability and aggregation of RBCs in a concentration-dependent

way, but it is not likely to cause cell death or hemolysis [86]. Size also matters in the ND-RBC interactions, as small NDs (5 nm) penetrated into RBCs, while larger NDs (100 nm) were localized on the RBC surface (Figure 4) [86].

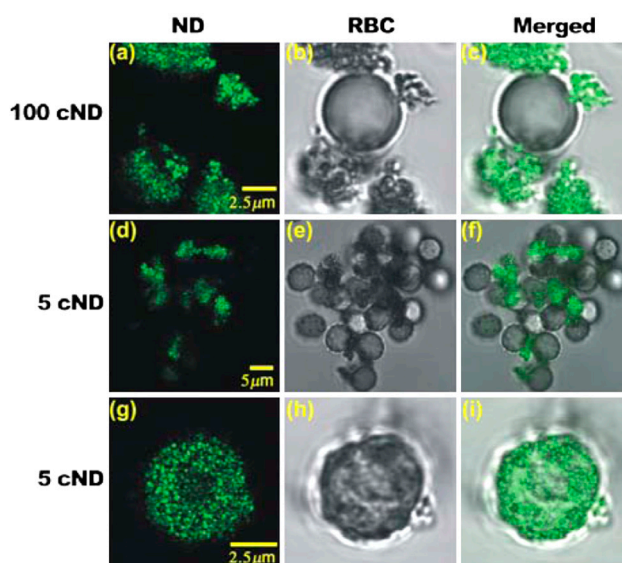


Figure 4. Nanodiamond interaction with human RBCs. Fluorescence (a,d,g), bright field (b,e,h) and merged optical microscopy images (c,f,i) of 100 nm (a–c) and 5 nm (d–i) nanodiamond particles. The images show larger NDs (100 nm) attaching to the cell membrane and smaller NDs (5 nm) penetrating inside the erythrocytes. Reproduced with permission from [86].

The oxygenation state of both human and rat RBCs was not affected by in vitro exposition to NDs at concentrations below 100 $\mu\text{g}/\text{mL}$ and albumin adsorption contributed to reduce ND aggregation. [87]. In vivo, NDs were found to attach to RBC membrane and circulate in the blood stream up to 30 min without inducing any significant immune response [87].

An extensive in vivo study including blood, urine and histopathologic screening was performed in large animal models to investigate the biocompatibility of unmodified and doxorubicin-conjugated detonated NDs [88]. The results of hematological and coagulation test showed that ND-treated rats did not experience severe systemic inflammation or massive coagulation, while in non-human primates the RBCs count, distribution width, and mean corpuscular hemoglobin concentration revealed some fluctuations consistent with the standard reference levels. Since no significant alteration in the physiological parameters were directly attributable to ND administration, the authors concluded that NDs were well-tolerated at clinically relevant doses [88].

Although the research studies conducted so far are still incomplete, current results generally suggest a promising response of bare and charged NDs following contact with blood. The variability in the hemocompatibility response is likely to depend on the physicochemical properties, on the surface functionalization and on the presence of graphitic residuals and other surface contaminants resulting from the synthesis and purification processes.

4. Fullerenes

Fullerenes represent a family of carbon allotropes with cage-like fused-ring icosahedral structure. C₆₀ is the most common form of carbon fullerene (CF), consisting of 20 hexagonal and 12 pentagonal rings arranged in a symmetric closed cage structure. Its discovery, in 1985, earned the Nobel Prize for Chemistry to its pioneers Kroto, Curl, and Smalley. Since then, CFs have raised the attention of researchers in various scientific fields, including nanomedicine, as they have shown unique properties such as tensile strength, electrochemical properties, thermal- and photo-conductivity [89].

A comprehensive review of CFs properties, synthesis, and functionalization methods, as well as biomedical applications, can be found in the work from Goodarzi et al., which is summarizing the progress of fullerene research during 30 years since its first discovery [90]. Biomedical applications of fullerene derivatives include anti-retroviral drugs, photodynamic therapy, MRI contrast agents, and tumor therapy [91].

If on the one hand the antioxidant/cytoprotective potential of fullerenes and its derivatives has been considered for the prevention of oxidative damage [92], on the other hand concerns have been raised about the biocompatibility of CF. Potential oxidative, genotoxic, and cytotoxic responses to CFs have been reported [29,93,94], surface derivatization being one of the key factors driving the biological response [95,96]. Due to its hydrophobic nature, in fact, bare CF presents an elevated cytotoxicity [91] and needs to be modified for improving its originally poor solubility in polar solvents and to acquire specific functions.

To date, the scientific literature on protein adsorption and hemocompatibility of CFs is fragmentary and only a few research studies dealing with the interactions between specific types of CFs and individual blood components have been reported. A recent study analyzed the effects of fullereneol (C₆₀(OH)₄₄) following incubation with some of the most abundant serum proteins, i.e., BSA and γ -globulins, showing that the proteins bound to fullereneols with similar affinity degree and without any significant change in their conformation (Figure 5) [97]. Such a binding resulted in favorable biological implications, as it decreased the cytotoxicity of fullereneol nanoparticles in GES-1 cell lines. Protein adsorption on CF surfaces also seems to form a protective layer preventing salt-induced coagulation in PBS, thus enhancing NP stability in the physiological environment [98].

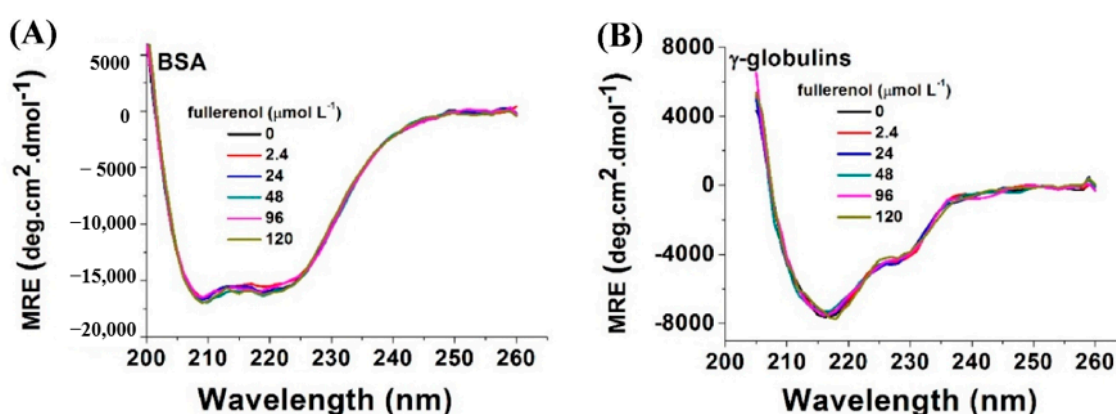


Figure 5. CD spectra of BSA (A) and γ -globulins (B) in the presence of different concentrations of fullereneol. With the addition of fullereneol the characteristic bands of BSA and γ -globulins did not show significant changes, suggesting that fullereneol did not induce any perturbations in the protein secondary structure. Reprinted from [97], with permission from Elsevier.

Prolonged bleeding times and inhibition of thrombosis in Sprague–Dawley rats following fullereneol injection were observed recently by Xia and colleagues [99]. Despite their negative surface charge, the polyhydroxylated derivatives of fullerene did not induce platelet activation or aggregation *in vitro* and delayed the coagulation *in vivo* by inhibiting the activity of thrombin and activated coagulation factor X (FXa). Hydrated C₆₀ fullerene at super-small concentrations (10^{-12} – 10^{-14} M) influenced the kinetics of clot lysis accelerating fibrinolytic reactions *in vitro* [100]. This effect was attributed to the capability of hydrated C₆₀ to induce ordered aqueous structures that contribute to stabilize protease molecules, rather than to the direct effect of C₆₀ particles. CFs seem thus to regulate water-protein and protein-protein interactions in the case of tissue plasminogen activator (t-PA) factor. Whether the same stabilizing effect could be elicited *in vivo* or with different kinds of serum proteins has not yet been investigated.

The mechanical characteristics of human RBC membrane were found to change following contact with C60 fullerene. In particular, the tensile resistance of the lipidic bilayer decreases significantly with increasing C60 concentration, as proven by both experimental data and theoretical simulations based on a mechanical model [101]. This effect, combined with evidence showing the ability of C60 to infiltrate into lipidic bilayers [102], suggested that CFs may significantly affect blood cells. Dose- and time-dependent modifications of erythrocyte membrane, including shrinkage and increase of surface roughness, were observed following incubation with C60 nanoparticles prepared by solvent exchange using tetrahydrofuran [103] and the effect was related to hemolysis and increase of ROS production. On the other hand, Avilova et al. showed by means of NMR spectroscopy techniques that amphiphilic water-soluble CF derivatives were trapped on the RBC surface or inside the membrane [104]. Strong interaction with human erythrocyte membrane was also revealed in the case of an organophosphonate fullerene, which induced dose- and irradiation-dependent lipid peroxidation mediated by reactive oxygen species, including superoxide radical and, to a major extent, hydroxyl radical and singlet oxygen [105]. Although there are no univocal values defining the concentration threshold for inducing hemolysis, it is clear that the hemolytic action induced by CFs increases as the dose increases. The hemolytic effect of fullerene and its derivatives seems to depend on synthesis methods, complexation agents [103], and surface structure, with greater hemolytic activity induced by cationic chains rather than by neutral or anionic terminations [106].

5. Carbon Dots

Carbon dots, a class of CNs less than 10 nm in size, were discovered accidentally in 2004 during electrophoretic purification of SWNTs [107] and immediately showed attractive properties, first of all photoluminescence (PL), as well as rapid electron transfer capability, and physical and chemical stability. Both top-down (arc discharge, laser ablation, and electrochemical oxidation) and bottom-up (thermal/combustion, supported synthetic, or microwaves) approaches can be used to synthesize CDs [108]. Depending on the method used for the synthesis, different structures can be obtained, which may include a crystalline or amorphous core surrounded by a polar or apolar shell [109]. Quasi-spherical graphitic, presenting a graphitic core composed of sp^2 -hybridized carbon layers, are the most common type of CDs, but more recently other types of carbon dots with PL properties have been produced with a core based on amorphous carbon, graphene or carbon nitride structures, either in a graphitic- or b-crystalline arrangement (g-C₃N₄ or b-C₃N₄) [109]. The synthesis process is followed by passivation (often necessary to obtain highly fluorescent CDs) and purification/separation steps, which lead to particles with a high degree of carboxylic groups on the surface. This contributes to good solubility and colloidal stability in water and allows for an easy surface functionalization with various organic, inorganic, or biological moieties. Due to their extraordinary optical properties and low toxicity, as demonstrated both *in vitro* and *in vivo* [110–112], CDs main applications are in the field of cell labeling, bioimaging, and sensing [113–115].

Very few information is available at present on the hemocompatibility of this novel class of CNs. The only comprehensive study on CDs hemocompatibility was published by Li and colleagues and was based on CDs (diam < 10 nm) synthesized by hydrothermal carbonization of α -cyclodextrin [116]. In this work, the authors performed a broad series of *in vitro* and *in vivo* experiments to elucidate the effects of the fluorescent CDs on blood cells (RBC morphology and lysis), platelets, complement system, and coagulation. Interestingly, they found that all blood components were affected in a dose-dependent manner by contact with CDs. In particular, CD concentrations of 0.01 mg/mL and 0.1 mg/mL preserved the physiological RBCs morphology, while higher concentrations (from 1 mg/mL to 10 mg/mL) induced an increasing degree of RBCs deformation and hemolysis accompanied by hemoglobin release (Figure 6). Hydrophobic interactions seem to drive the CD-RBC interactions guiding the subsequent deformation and lysis of the RBCs membranes.

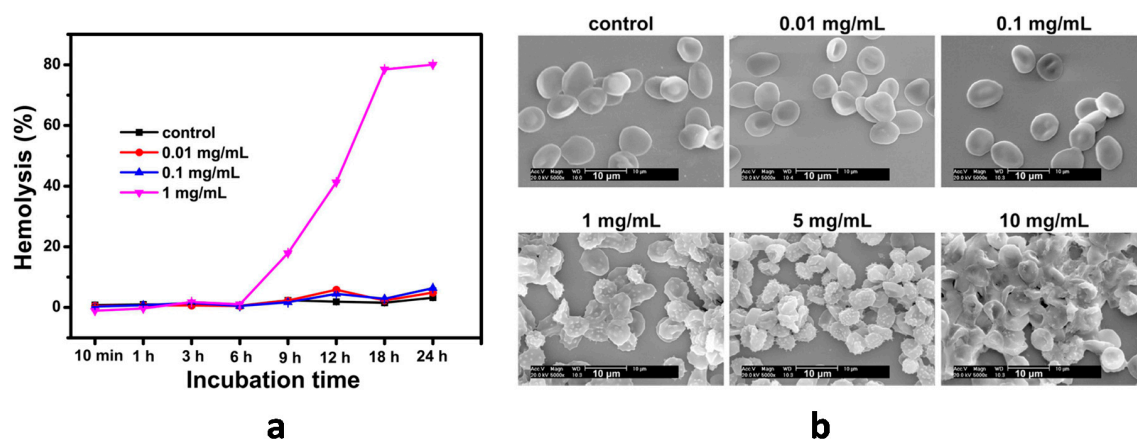


Figure 6. (a) Hemolysis ratio of RBCs induced by fluorescent carbon dots with different concentrations. (b) SEM images showing the morphology and aggregation of RBCs incubated with the fluorescent carbon dots at different concentrations. Reprinted with permission from [116]. Copyright 2015 American Chemical Society.

The same CDs derived from α -cyclodextrin were tested against blood coagulation *in vitro* and *in vivo*. At low CD concentration (0.1 mg/mL) aPTT and PT did not show significant variations respect to control PBS solution, while at concentrations of 1 and 2 mg/mL significantly higher values of aPTT and PT were measured, indicating a potential anticoagulant activity. No significant effects on blood clotting strength and complement activation were registered up to 1 mg/mL CDs. On the contrary, the CDs at 0.01 and 0.1 mg/mL caused a significant expression of P-selection on the thrombocyte membrane, which refers to platelet activation [116]. Although this experimental work presents some inconsistencies in the sampling spots, it represents the baseline for hemocompatibility studies on CDs, and finally suggests that the effects of CDs are strongly related to particle concentration. In this specific case, most of the parameters affecting blood compatibility were within the normal range until the CD concentration remained below 1 mg/mL, while several adverse effects were shown at higher CD concentration [116]. The same authors showed promising biocompatibility properties of fluorescent CDs conjugated with hyperbranched polyglycerol, which had improved performances in terms of RBCs morphology and hemolysis respect to bare unmodified CDs [117]. Minimum RBC toxicity and negligible hemolytic effect were confirmed by different experimental *in vitro* studies with CDs at concentration up to 2.0 mg/mL [118,119], while only slight effects were observed on the α -helix structure of BSA following incubation with CDs derived from sugarcane molasses [119]. An *in vivo* toxicology testing showed normal values for the hematology parameters, including white blood cells, red blood cells, hemoglobin concentration, and platelet count following CDs injection in female Balb/c mice over 90 days [17]. Moreover, little cytotoxicity on mouse embryonic fibroblasts and no blood coagulation or RBC aggregation effect were enhanced in mice treated with cationic CDs [120].

Much work is still required in order to better clarify the fate of CDs exposed to blood and specific responses need to be evaluated on a case-by-case basis considering the origin, synthesis process, and surface chemistry of the different types of CDs.

6. Carbon Nanotubes

Carbon nanotubes in their simplest form, i.e., single-wall carbon nanotubes (SWCNTs), consist of a single sheet of graphene rolled up in a seamless tubular form with a diameter of a few nanometers and typical length in the range of a few micrometers [121,122]. They were discovered in 1993 by the same research group that a couple of years earlier identified, for the first time by electron microscopy, what they called “multi-walled carbon nanotubes” (MWCNTs), complex structures formed by two or more graphene cylinders aligned concentrically along the main axis [123]. Significant improvements have been reached over the years in the synthesis, characterization, and functionalization of CNTs, allowing

for a more massive production of nanotubes with increased quality in terms of purity, dimension and chirality control, surface chemistry, and dispersibility in aqueous media. Exceptional length/diameter aspect ratio (up to 10^7), mechanical strength, and chemical and thermal stability [122], heat conduction, gas adsorption, and semiconducting behavior are some of the special properties that encourage the use of CNTs in a range of applications. In the biomedical field, the peculiarities of CNTs have been exploited to develop temperature- or pH-triggered delivery systems for proteins, DNA, anticancer drugs [124], or vaccines [125], or to improve the structural and electrical characteristics of composite scaffolds for bone, myocardium, or neural tissue engineering [126]. Moreover, CNTs have been used to produce sensors for glucose, cancer biomarkers, and nucleic acids [8], as well as patterned surfaces for stimulating cell growth and differentiation.

CNTs have shown tremendous potential for biomedical applications and for this reason they have been studied more extensively than other CNs in terms of biological response and hemocompatibility. However, the toxicity of CNTs is still a controversial issue. Contrasting outcomes have been found, depending on sample geometry, dimensions, presence of impurities, as well as surface chemistry and functionalization [127,128]. The topic of CNT biocompatibility opens a broad chapter that still does not offer definitive answers, and which we cannot discuss here for the sake of brevity.

Numerous literature studies have examined the different aspects involved in the interaction of SW- and MW-CNTs with blood. Several spectroscopic and molecular modeling approaches have been used to characterize protein adsorption from single protein solution or from more complex mixtures, blood serum or plasma, laying the groundwork for a better understanding of the molecular basis of CNT-protein interactions. In general, experimental investigations have shown that protein adsorption is a spontaneous process taking place when CNTs are immersed in a physiological fluid and that the formation of a protein corona at the nanoscale depends on the combination of several factors related to the properties of both nanomaterials (e.g., curvature, aspect ratio, presence of functional moieties) and proteins (e.g., structure, presence of hydrophilic/hydrophobic domains, aromatic or charged amino acids) [28,129]. It has also emerged that the process of adsorption to CNT surface leads, in most of the cases, to protein denaturation. Different types of intermolecular forces can favor protein binding to CNTs. In particular, hydrophobic interactions seem to play a central role thanks to their additive effect that involves multiple contact points between the CNTs and the hydrophobic domains of the proteins in an attempt to minimize exposure to the hydrophilic environment [130]. Amphiphilic protein molecules can surround the CNTs by turning their hydrophobic residues towards the tubes and exposing their hydrophilic domains to the aqueous media. Hydrogen bonding and electrostatic forces are also actively involved in the protein corona formation [131,132], while π - π stacking interactions can occur between the aromatic rings in the CNT structure and aromatic amino acids (histidine, tryptophan, and, to a minor extent, phenylalanine) [130]. Experimental analyses based on single protein solutions showed that both pristine and surface-modified SWCNTs and MWCNTs incubated with BSA can form stable bioconjugates with protein molecules. Nonspecific electrostatic interactions dominate in the case of MWCNTs [133], while also hydrophobic interactions [134] and π - π stacking participate to BSA-CNT bond in the case of carboxylated CNTs (Figure 7) [135]. BSA molecules are significantly destabilized by the interactions with CNTs and substantial structural changes can arise in the protein secondary and tertiary structure [135–138]. A decrease by 14.06% in the content of the alpha-helix structure was measured, for example, in BSA exposed to COOH-SWCNTs [134].

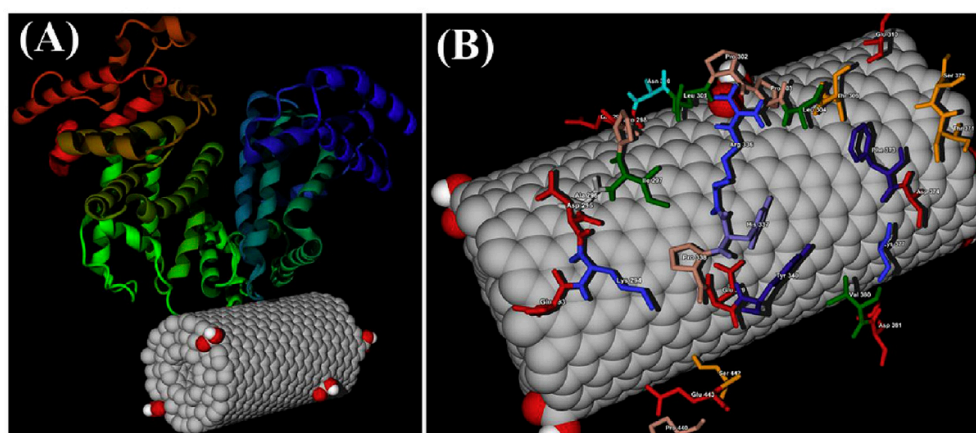


Figure 7. Predicted binding model of BSA molecule on COOH-MWCNTs. (A) Lowest docking energy conformation; (B) amino acid residues involved in binding interactions. According to the model, 29 amino acid residues of domain II of BSA took part in the binding interactions of BSA with COOH-MWCNTs. The presence of hydrophobic (Ala, Leu, Pro, Phe, and Val) and aromatic (Tyr and Phe) residues suggested that the binding forces between BSA and COOH-MWCNTs include hydrophobic and π - π stacking interactions. Reprinted from [135], with permission from Elsevier.

The study of the influence of CNT geometric features on protein adsorption lead to discordant findings with some authors demonstrating stronger BSA adsorption and molecular unfolding on small CNTs with large surface area [139], and some other showing an inverse relationship between BSA protein adsorption and surface curvature [140].

Protein adsorption experiments from single protein solutions often represent oversimplified systems that differ from real physiological conditions. In biological fluids, in fact, the competition between different proteins is a significant phenomenon and the access to specific regions of a given protein species could be influenced by other species in the mix. Blood plasma, in particular, includes hundreds of proteins in a wide range of MW and with different specific functions. An extensive analysis of protein adsorption from human blood plasma on different MWCNTs functionalized by carboxyl- and ammonium-groups was recently published by Nicoletti et al. [141]. By means of mass spectrometric analysis, the authors were able to detect the characteristic patterns of proteins adsorbed on pristine and functionalized CNTs, revealing a high affinity of proteins for CNTs. The absence of any significant differences in the composition of hydrophobic, basic or acidic residues of bound proteins led the scientists to exclude any correlation between the chemical functionalization of CNTs and the primary sequence of adsorbed proteins. Selective adsorption of IgG and enrichment of some low-abundant plasma proteins as apolipoproteins and complement components, were enhanced on MWCNTs [141], in agreement with previous studies [142]. According to De Paoli et al., Fng, has, and IgG are among the main components forming the protein corona on COOH-MWCNTs after incubation with human plasma, together with other relatively abundant proteins like hemoglobin, blood coagulation factors, and proteins related to complement and immune systems [131]. Coagulation proteins, IgG, apolipoproteins, and proteins of the complement system were also found to bind PEG-SWCNTs modified with 2 kDa MW polyethylene glycol chains [143]. Due to their small size, low molecular weight proteins (<54 kDa) seem to have a strong binding affinity for MWCNTs [144]. However, despite its large molecular dimensions (340 kDa MW and 45 nm length ca.), fibrinogen showed selective binding capacity to DWCNTs [145] and MWCNTs [131] as well as unexpectedly higher binding affinity to SWCNT respect to albumin [146]. HSA, the most abundant protein in blood, was preferentially adsorbed on pristine SWCNTs following incubation with human plasma or serum [147], but it did not present specific affinity for surface-modified CNTs [148].

Although it is difficult to draw general conclusions, CNTs have often been found to interfere with proteins inducing conformational changes. Modification of the secondary and tertiary structure

was registered for albumin [134–137,139] hemoglobin, myoglobin [149], and other proteins [131,150]. The extent of this effect is a critical parameter to be investigated, since conformational alterations could lead to severe modification of protein functionality or affect the subsequent interactions of the CNT-protein system with cells, platelets, and other biological components, finally determining the fate of the nanotubes in the biological system [129]. The adsorption of complement components to carbon nanosurfaces and modification of their structural configuration may lead to the activation of the complement system and consequently induce inflammation, granuloma formation, or other side effects, such as acute allergic-like reactions and anaphylaxis [151,152]. Investigating the consumption of the complement system from human serum by single- and double-walled CNTs, Salvador-Morales et al. showed that all the types of CNTs tested activated the complement system in a dose-dependent manner via both classical and alternative pathways, with dominance of the classical pathway related to C1q binding in the case of SWCNTs [145]. Conversely, direct binding of C1q and C1s-C1r-C1r-C1s catalytic subunit was detected by TEM imaging on MWCNTs but not on SWCNTs [153]. C1q and C1s-C1r-C1r-C1s were tidily distributed on the side walls of MWCNTs, but no evidence of activation of the C1q complex was found. In a recent quantitative analysis, the complement components C1, C4a and C4b have been identified in the protein corona of COOH- and N-functionalized MWCNTs, confirming the potential of MWCNTs to activate the complement system via the classical and alternative pathways and suggesting a possible role of CNTs as initiators of local inflammatory reaction via the C4a component [141]. Moreover, the consumption of C3 and C5 (which is a marker of MAC-Membrane Attack Complex formation) was registered following incubation of both pristine and derivatized CNTs in human serum (Figure 8) [154]. As the products of complement activation (i.e., C3b, C4b, iC3b, C3d, etc.) may act as adjuvants in the immune response to foreign materials and trigger phagocytosis and effector cytokine response, the potential of CNTs to activate the complement system is a cause of concern for possible adverse responses, like inflammation and granuloma formation [155]. Attempts to modify CNT surface by pre-absorption of proteins (e.g., HSA) or immobilization of molecules (e.g., PEG) have shown potential reduction but not complete exclusion of complement system activation [151,156,157].

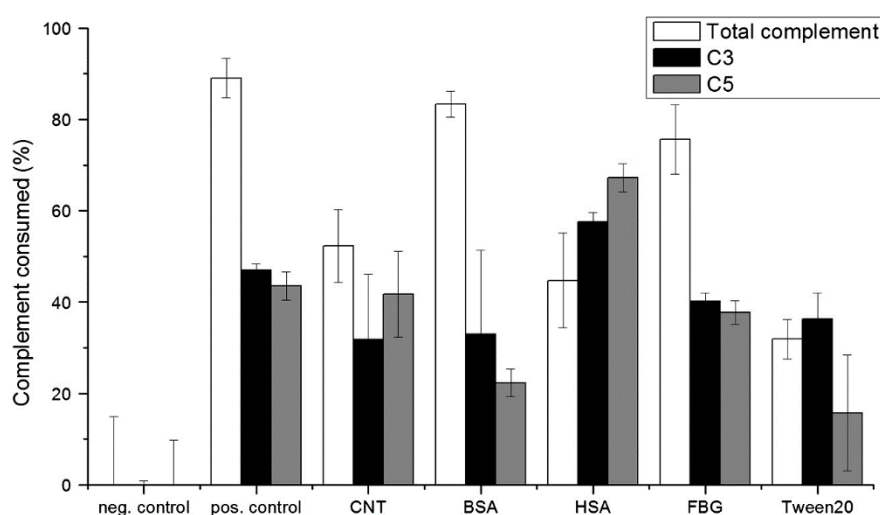


Figure 8. Complement consumption for total complement and C3 and C5 components induced by double walled-CNTs (DWCNTs)—pristine or coated with various plasma proteins (BSA, HSA, FBG) or Tween 20. All the CNT samples tested activated complement predominantly through the classical pathway and consumption up to C5 indicated potential formation of the Membrane Attack Complex. Reprinted from [154], with permission from Elsevier.

The thrombogenic potential of CNTs has been studied both *in vitro* and *in vivo*. Burke et al. analyzed the thrombogenic behavior of pristine, COOH- and NH₂-functionalized MWCNTs, reporting *in vitro* activation of the intrinsic coagulation cascade as measured by aPTT assays [158]. This effect

was influenced by CNTs functionalization, with carboxylated nanotubes presenting the highest prothrombotic capacity. Specific interaction of functionalized MWCNTs with factor IXa and stimulation of its enzymatic activity may be the mechanisms contributing to accelerate the propagation of the intrinsic clotting cascade [158]. Activation of the coagulation system through the contact pathway was instead hypothesized by Sokolov et al., who showed that carboxylated SWCNTs significantly shortened the clot formation time in whole plasma, but not in plasma lacking the coagulation factor XI [159]. In some cases, the analysis of CNT-related thrombosis produced different outcomes depending on whether the tests were conducted in vitro or in vivo. For example, in the study of Burke et al., platelet activation in vitro was triggered by NH₂-MWCNTs rather than by pristine or COOH-MWCNT, while pristine MWCNTs induced higher pro-coagulant activity when injected in mice, as related to decreased platelet counts and increased von Willebrand Factor (vWF) and D-dimer levels [158]. Prothrombotic activity of SWCNTs and MWCNTs, even at low doses, was demonstrated by several in vivo studies considering systemic administration in rodent animal models [160–163].

The potential of pristine MWCNTs to induce platelet activation and aggregation was reported by Semberova et al., who also showed considerable release of platelet-derived microparticles (PMPs), i.e., membrane vesicles with marked procoagulant activity [164]. The same authors demonstrated that the mechanisms underlying platelet activation by CNTs involve extracellular Ca²⁺ influx. However, modification of intracellular Ca²⁺ levels were not related to any damage in the platelet plasma membrane, but rather to store-operated Ca²⁺ entry [165]. In a later study, the same research group proved a strong effect of the protein species forming the CNT corona on blood platelet [131]. Bare carboxylated MWCNTs induced the activation of PLTs and release of PMPs, while the pre-adsorption of IgG molecules minimized PLT aggregation, although inducing PLTs fragmentation and PMP release. On the other side, the adsorption of HSA and, to a lower extent, Fng on COOH-MWCNTs did not affect platelets morpho/functional characteristics and attenuated PLT aggregation. It was also observed that the highly alkaline plasma protein histone H1 adsorbed to COOH-CNTs caused significant damage to PLTs membrane, PMPs production and PLT aggregation even at higher level than uncoated COOH-CNT [131]. A larger degree of platelet activation was achieved by functionalized long MWCNTs compared to short ones, with a marked reduction in platelet viability induced by long NH₂-MWCNTs (Figure 9) [166]. CNTs affected blood coagulation by shortening the fibrin clot formation times and inducing hardening (long NH₂-MWCNTs) or softening (long COOH-MWCNTs and short NH₂-MWCNTs) of the blood clot, respectively [166].

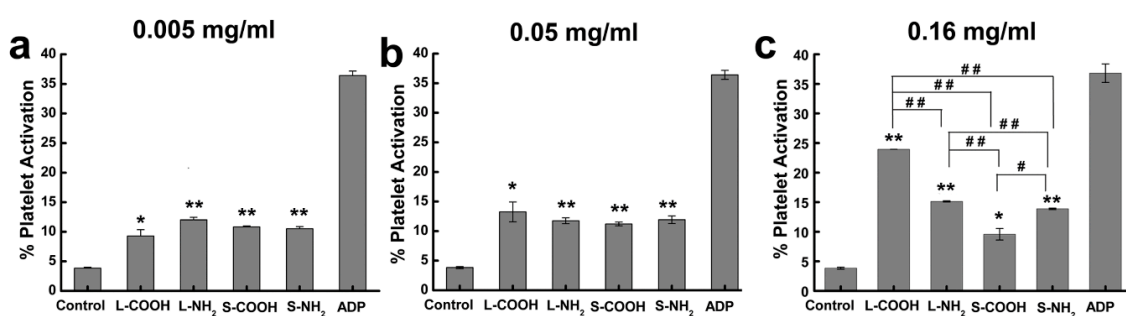


Figure 9. Platelet activation induced by four different types of functionalized CNTs, including long (L) and short (S) MWCNTs at different concentrations: 0.005 mg/ml (a), 0.05 mg/ml (b) and 0.16 mg/ml (c). Dose-dependent platelet activation was observed. At the highest concentration (c), long L-COOH and L-NH₂ induced higher level of platelet activation than S-COOH and S-NH₂, respectively. *: significant difference from the negative control (* $p < 0.05$, ** $p < 0.01$); #: significant difference between the indicated MWCNTs (# $p < 0.05$, ## $p < 0.01$). Reprinted with permission from [166].

Pristine and functionalized (CONH₂-; COOH-; OH-; and PEG-) SWCNTs were shown to activate platelets and to promote platelet-granulocyte complex formation with different intensity in human whole blood [162,167] with exception of OH-SWCNTs. PEG-coated SWCNTs presented the highest

platelet activation and aggregation capacity, as well as abundant formation of PLT-granulocyte complex. This result is quite surprising, considering that PEGylation is a common strategy used for improving the biocompatibility of NP and reducing their potential recognition from the mononuclear phagocyte system [168]. PLT activation and PLT-granulocyte formation were supposed to be related to a lower degree of HSA adsorption to PEGylated SWCNTs respect to other functionalized CNTs, as supported by the thesis of Vakhrusheva et al., which suggested a protective effect of adsorbed HSA against platelet activation [169]. P-selectin expression and formation of platelet-granulocyte complexes following contact with SWCNTs was confirmed by other *in vivo* measurements [163]. AFM imaging evidenced effective protein binding on the sidewalls of PEG-SWCNTs following incubation with HSA, Fng and IgG [170]. These three test proteins were adsorbed to PEG-SWCNTs in comparable amounts, despite having different concentration in plasma. Relatively high concentration of adsorbed Fng and IgG may, thus, play a significant role in platelet aggregation and activation of neutrophils when PEG-SWCNTs are exposed to blood. PEG-SWCNTs caused dose- and time-dependent activation of neutrophils in blood. In particular, the levels of neutrophil activation markers and oxidative stress for IgG-treated CNTs were about double if compared to untreated PEG-SWCNTs [170], supporting the hypothesis that adsorbed IgG may affect neutrophil response to PEG-SWCNTs.

Carbon nanotubes in their pristine form or with covalent (e.g., amine, alcohol, carboxylate) or non-covalent (e.g., PEG) surface modifications showed no hemolytic activity in the study of Canapè et al. [171]. *In vitro* analyses showed that SWCNT, and in particular oxidized SWCNT, were not internalized by RBCs even at relatively high doses and did not induce hemolysis or toxic effects on human RBCs [172]. On the other hand, acid functionalization of SWCNTs caused nanoparticle uptake by murine erythrocytes *in vivo*, as well as externalization of phosphatidylserine (an early marker of apoptosis and cell death) on RBCs membrane and dose- and time-dependent hemolysis in mice [173]. Further adverse effects, like sustained anemia following administration of poly-dispersed acid-functionalized SWCNTs, have been registered in mice and related to the uptake of acid-functionalized SWCNTs by early precursors of erythroid differentiation [174].

CNT dispersion seems to be a factor influencing their hemocompatibility, as proven by a recent study showing that bundled SWCNTs had higher hemolytic activity respect to dispersed SWCNTs and induced significant modifications of RBC shape and fusion [175].

In conclusion, CNT thrombogenic potential still represents a critical issue for drug delivery and other biomedical applications, and the strategies adopted till now to modify CNT surface are only minimally effective in preventing adverse thrombotic events. Although numerous literature studies on CNT interaction with blood components are currently available, no definitive answer has been found so far and further efforts need to be devoted to providing a complete and comprehensive answer on CNTs hemocompatibility.

7. Graphene-Based Nanostructures

Graphene is a relatively novel material, consisting of a single layer of sp^2 -hybridized carbon atoms arranged in a regular honeycomb structure. Its discovery took place in 2004 at the laboratories of the University of Manchester by A. K. Geim and K. S. Novoselov and rapidly gained an exceptional resonance in the field of materials science, so that in 2010 the authors were awarded the Nobel Prize in Physics [176]. Besides being by far the first 2D material ever isolated, graphene has unique properties due to its structure and electronic spectrum. Graphene has in fact excellent mechanical characteristics, with an elastic modulus that approaches 1 TPa and fracture strength of 130 GPa [177], theoretical specific surface area of 2630 m^2/g , and high electrical and thermal conductivity combined with optical properties [178,179].

Graphene oxide (GO) and reduced graphene oxide (rGO) are oxidized analogues of graphene with some discontinuities in the hexagonal lattice due to a variable portion of oxygen-based functional groups. GO is characterized by the presence of hydroxyl and epoxy-like groups in the basal plane as well as mainly carbonyl and carboxyl groups at the sheet edges [180]. rGO can be obtained by

chemical, thermal, or electrochemical reduction of GO, and has a final structure similar to graphene, with a much lower content of oxygen functional groups with respect to GO. Different methods of preparation and processing can lead to graphene derivatives with a variable degree of oxygenation. Unlike graphene, GO has a hydrophilic character and can be easily dispersed in water and other polar solvents with long-term stability thanks to the presence of polar (-OH, -O-) and charged (-COO⁻) oxygen-rich groups [181]. The presence of active chemical groups and of surface free π electrons allows the formation of both covalent and ionic bonds, hydrogen and π - π interactions, and makes the GO sheets easy to functionalize, with special attractiveness in the biomedical field. A series of biomolecules can thus be immobilized to GO surface to improve its colloidal stability, to reduce possible toxic effects and to impart GO with diagnostic or therapeutic capabilities [182]. The impact of the discovery of graphene and its derivatives after only 15 years is noteworthy, as many applications in different fields of technology have been proposed to date, like electronic devices (e.g., transparent conductors and ultrafast transistors) and high-performance materials for energy generation and storage. A number of graphene-based applications have also been proposed in the biomedical field [183], including drug and gene delivery [182,184], photodynamic and photothermal therapy [185–188], bioimaging [189], and biosensing [190,191]. Graphene-based materials also exhibited attractive antimicrobial activity [192] and several interesting approaches have included graphene or graphene composites as scaffolds for tissue engineering and regenerative medicine with applications including nerve, bone, cartilage, skeletal muscle, skin, and myocardium [193,194].

Due to the nature of graphene-based materials it is possible to assume that the interaction of graphene and rGO with blood proteins is dominated by weak interactions, including hydrophobic interactions and π - π stacking. On the other hand, the abundance of reactive functional groups on GO enables protein adsorption through a synergistic effect involving covalent and non-covalent bonds [195]. Different peptides, proteins and enzymes (e.g., HRP, heparin, polylysine, etc.) have been immobilized on GO surface via direct binding to intrinsic surface functional groups, π - π stacking, and/or hydrophobic interactions [195], showing extreme easiness of protein adsorption to GO surfaces. The interaction of graphene and GO with single proteins has been assessed in terms of binding affinity, action mechanisms, as well as conformational and functional modifications. A recent study considered albumin adsorption to four different types of nanosheets, including pristine GO or GO sheets modified by carboxylic groups (COOH), polyethylenimine (PEI), and chitosan (CS), showing that HSA was readily adsorbed to the GO-based sheets with a higher affinity for pristine GO, followed by COOH-GO, CS-GO, and PEI-GO in that order [196]. From isothermal titration calorimetry analysis, it was concluded that HSA interacted with GO and COOH-GO mainly via hydrogen bonding, while hydrophobic interactions contributed to HSA adsorption to PEI-GO and CS-GO surfaces. Moreover, the authors suggested that GO affected HSA functionality by blocking the protein active sites or destroying its original structure [196]. Kenry et al. investigated the molecular interaction of GO sheets with lateral size distribution in the range between 0.280 μm and 4.138 μm with three of the most abundant human blood plasma proteins, namely HSA, Fng, and γ -IgG. Interestingly, protein adsorption showed a clear size-dependent behavior, with HSA adsorption increasing and Fng decreasing linearly with increasing GO mean lateral size (Figure 10) [62]. Based on these results, large GO nanosheets may, thus, have better hemocompatibility compared to smaller ones, due to a higher albumin-to-fibrinogen adsorption ratio. Quantitative parameters describing plasma protein binding to GO (i.e., quenching efficiency, association and dissociation constants, and binding cooperativity) were obtained from the spectroscopic analysis of protein fluorescence quenching induced by GO with different lateral dimensions. The data suggested the occurrence of direct interactions between GO and chromophore residues (tryptophan, tyrosine, phenylalanine) in the three proteins investigated, as well as possible conformational changes [62], in agreement with previous studies [197].

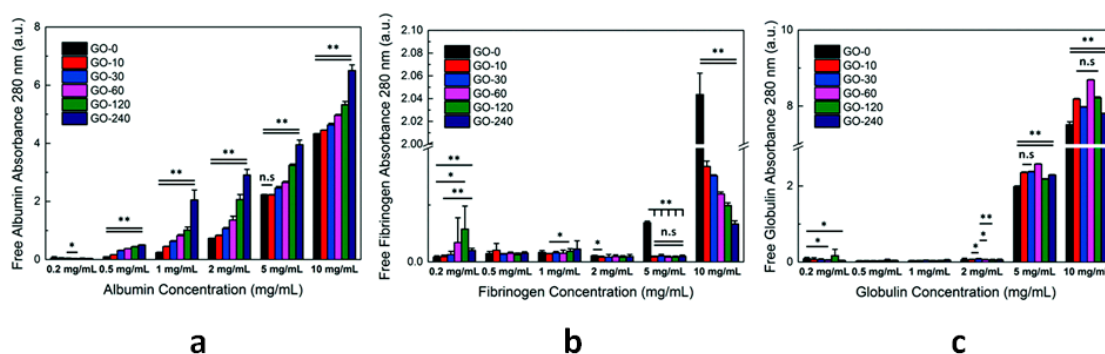


Figure 10. Absorbance of free plasma proteins (albumin (a), fibrinogen (b), and globulin (c)) following incubation with GO nanosheets with different lateral sizes. The * on double horizontal bars denotes statistically significant differences among all samples for $p < 0.05$. The ** on single horizontal bars indicate statistically significant differences for two specific samples being compared for $p < 0.1$ and 0.05 , respectively, while n.s denotes statistically not significant. The absorption of the different protein species depends on the size and concentration of GO. Adapted with permission from [62]—Published by The Royal Society of Chemistry.

Dose-dependent quenching of serum protein intrinsic fluorescence was confirmed to take place upon interaction with GO, with higher adsorption efficiency at lower nanosheet concentration. Moreover, higher adsorption efficacy was found for GO with respect to rGO [198]. Conformational studies proved that HSA structure was preserved following exposure to GO sheets, while an increasing effect on Fng secondary structure was enhanced with increasing GO concentration from 20 mg/mL upwards [62]. The same authors proved that albumin was irreversibly adsorbed to GO and maintained its passivating properties, contributing to reduce blood clot formation [199]. The application of HSA-GO conjugates as antithrombotic surface coatings was therefore suggested. In a comparative study, Chong et al. analyzed the adsorption kinetics of GO (0.5–3 μm lateral dimension), rGO (0.5–3 μm lateral dimensions) and ultrapure SWCNTs (outer diameter $< 2\text{nm}$; 5–30 μm length) from four of the most abundant plasma proteins, including BSA, bovine serum Fng, immunoglobulin (Ig) and transferrin (Tf) [200]. They found that all the nanomaterials tested had preferential affinity for bovine Fng followed by Ig, Tf, and BSA in decreasing order. GO and rGO presented a much higher protein adsorption compared to SWCNTs, suggesting that proteins prefer flat graphene surfaces to curved CNTs. The four tested proteins underwent substantial changes in their secondary structure when adsorbed onto GO sheets and followed different adsorption models. BSA and Tf presented a uniform mode of adsorption that included the decrease in alpha-helical features and increase in beta-sheet content after 5 min of contact with GO, while Ig and Fng exhibited a heterogeneous adsorption pattern with radical changes in their CD spectra from 5 min to 60 min incubation time [200]. Molecular dynamics simulations supported the hypothesis that π - π stacking and hydrophobic interactions drive protein (bovine Fng) adsorption to GO surfaces (Figure 11) [200].

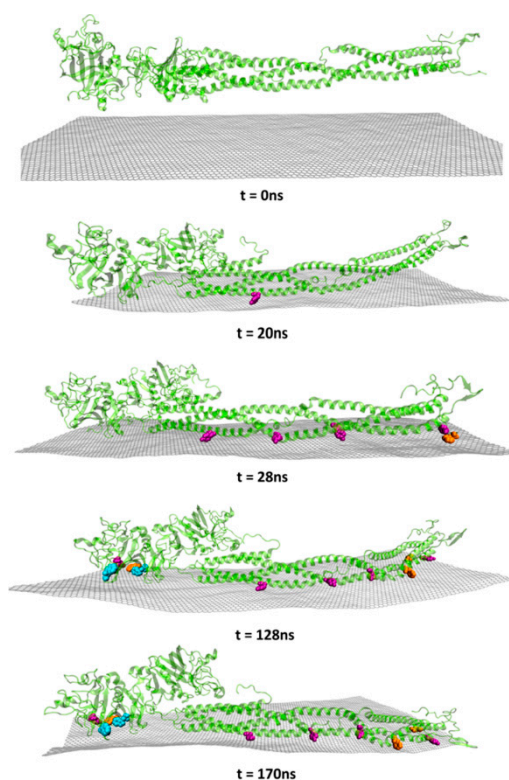


Figure 11. Simulated molecular adsorption dynamics of bovine Fng onto graphene surfaces. After initial contact, Fng molecules rearrange on the graphene surface due to hydrophobic interactions. The aromatics rings of protein amino acid residues Tyr (purple), Phe (orange), and Trp (blue) align with the graphene surface facilitating π - π stacking interactions. Reproduced with permission from [200]. Copyright 2015 American Chemical Society.

Conformational changes in the protein molecular structure following interaction with GO sheets have been confirmed by other literature studies based on fluorescence experiments and circular dichroism (CD). For example, Feng et al. showed that at low GO concentration (0.001–0.1 mg/mL) BSA was adsorbed maintaining mainly alpha-helix configuration, while at 0.5 mg/mL some modifications were induced in the BSA secondary structure. When GO was incubated with fibrinogen solution, the alpha-helix content of Fng molecules gradually decreased with increasing GO content, with evidence of structural changes when GO concentration was in the range from 0.05 to 0.5 mg/mL [201]. In a recent research paper, Castagnola and colleagues studied the protein corona adsorbed on the surface of graphene nanoflakes directly exfoliated and dispersed in human serum [202]. Besides demonstrating the stability of graphene dispersion in biological fluids, the authors documented by mass spectrometry that the major families of adsorbed proteins were lipoproteins (26%), albumin (10%), immunoglobulins (10%), hemoglobin (5%), and proteins of the complement (5%) and coagulation (3%) systems. Apolipoprotein A-I was the most abundant among the lipoproteins found in the corona and TEM analysis showed the availability of functional epitopes relevant in promoting specific recognition pathways (e.g., cell receptors) [202]. Mao et al. showed that albumin was the dominant component of the hard corona when graphene was incubated with low protein concentration, while some low MW proteins were enriched by graphene from protein mixtures at higher concentration [203]. High-MW proteins were reported to adsorb to pristine and reduced GO surfaces through hydrophobic interactions, while significant aggregation of rGO was supposed to be the cause of an unexpectedly less abundant adsorption on hydrophobic surfaces of more reduced GO [204].

Few studies in the literature considered the interaction of graphene derivatives with the complement system. It was suggested that GO can activate the complement cascade through calcium-sensitive pathways, as proven by dose-dependent increase of SC5b-9 and C4d in human

serum following exposure to GO [205]. Surface oxygen content significantly affected the degree of complement activation. Linear correlation was found between the levels of both C5a and SC5b-9 and the concentration of oxygen rich groups on GO surface when GO was tested in solution, while the opposite behavior was measured for immobilized GO [205]. Oxygen-dependent complement response was supposed to be due to a combination of surface functionalities and topographical changes on GO sheets. It was also demonstrated that GO in solution at concentration below complement activating threshold did not induce IL-6 release with protective effect against lipopolysaccharide-stimulated response in human blood leukocytes [205].

A protein coating inhibiting complement activation was obtained by non-covalent GO functionalization through spontaneous protein adsorption. In particular, GO surface modification with factor H (a complement regulatory protein) and albumin was effective in reducing GO-induced complement activation by 90% and 40%, respectively, if compared to pristine GO [206]. According to the authors, this strategy represents an effective way to improve GO properties to mask complement-activation and hinder adverse immune response. As regarding the immunotoxicity of graphene and its derivatives, a systematic review of the studies conducted *in vitro* and *in vivo* can be found in some recent comprehensive publications [207–209], which are considering the different aspects involved in defense mechanisms triggered by graphene-based materials on both the innate and adaptive immune system and the role of protein corona in guiding the interactions with immune cells.

The hemocompatibility of graphene, both pristine (hydrophobic) and functionalized by nitric acid treatment (hydrophilic), was analyzed by Sasidharan et al. [210]. The concentration of free hemoglobin in plasma following incubation with all the different graphene samples was significantly negligible compared to the positive control (Triton X-100), thus excluding the hemolytic effects of the graphene nanoparticles up to 75 $\mu\text{g}/\text{mL}$. Flow cytometry analysis showed the absence of P-selectin expression on platelet cell membrane, demonstrating that platelets are not activated by graphene, either pristine or functionalized with carboxyl, epoxy or hydroxyl groups [210]. Moreover, platelet count analysis enhanced no signs of platelet aggregation in graphene-treated human blood and PT and aPTT tests assessed the normal function of the coagulation system from both the extrinsic and intrinsic pathways. In summary, this paper showed that the tested graphene particles did not affect RBCs and did not interfere with platelet function and coagulation pathways, suggesting a non-thrombogenic behavior of pristine and functionalized graphene [210]. Concerns regarding GO hemocompatibility have been raised by Shingh et al., who revealed the prothrombotic behavior of GO both *in vitro* and *in vivo*. In particular, they showed that GO caused severe platelet aggregation *in vitro* through fibrinogen-mediated mechanisms and a less marked, though important, platelet activation effect [211]. Based on an *in vivo* thrombosis model, it has been confirmed that GO has a strong thrombogenic effect as it induced extensive pulmonary thromboembolism when injected intravenously into mice at 250 $\mu\text{g}/\text{kg}$ body weight. GO caused a significantly greater platelet aggregation level *in vivo* as compared to rGO, as well as a higher number of lung vessel occlusion, demonstrating the key role of surface charge distribution in platelet activation/aggregation and thrombotic response to graphene-based nanomaterials [211]. In another manuscript it was reported that the hemolytic ratio induced by GO suspension at the dosage of 10–80 $\mu\text{g}/\text{mL}$ was similar to PBS after 1 h incubation with RBCs. However, the hemolysis ratio was dose- and time-dependent, with maximum values around 20% after 6 h incubation with GO at a concentration of 80 $\mu\text{g}/\text{mL}$ [212]. Intravenous administration of GO in mice caused significant pathological changes in various tissues and organs when high doses (10 mg/kg body weight) were used, but not at lower doses (1 mg/kg body weight). Interestingly, GO exhibited long blood circulation time (half-time 5.3 ± 1.2 h) in comparison with other CNs [212]. In addition to showing dose-dependent hemolytic activity of graphene sheets and GO, Liao et al. found that smaller (sonicated) GO caused higher hemolysis respect to larger (untreated) ones (Figure 12), and that aggregated graphene sheets had lower detrimental effect on the erythrocytes in comparison to individually dispersed GO sheets with higher surface oxygen content [213].

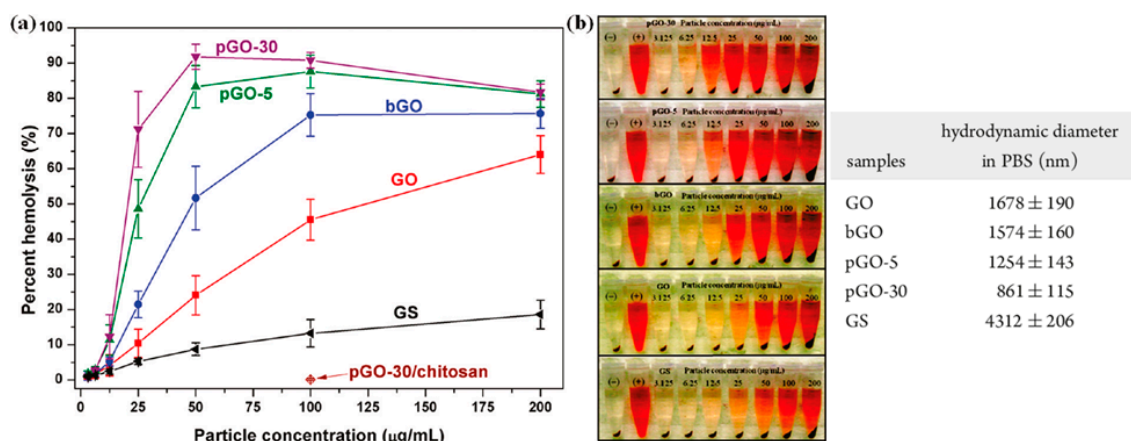


Figure 12. (a) Percent hemolysis of RBCs incubated with different concentrations of graphite oxide colloidal suspension obtained from Hummers' method (GO) and smaller graphene oxide obtained with sonication or hydrothermal processing (bGO, pGO-5, pGO-30, and GS). (b) Photographs of RBCs after exposure to the different GO samples, with red hemoglobin in the supernatant indicating the presence of RBCs with membrane damage. The hemolysis rate was dose- and size-dependent. Adapted with permission from [213]. Copyright 2011 American Chemical Society.

Recent studies of GO interactions with model and cell membranes have shown that GO interacts with neutral and negatively charged lipid membranes, leading to the rupture of neutral membrane vesicles but not of negatively charged ones. Coating GO with lipid membranes (e.g., phosphatidylcholine) was, thus, proposed as an effective strategy for decreasing the hemolytic effect of pristine GO [214].

Different factors have been reported to contribute to GBN-induced cell toxicity, including lateral size, surface structure, presence of sharp edges, surface charge, oxygen content, functionalization, presence of impurities and particle aggregation [215]. Similarly, the same factors can affect the interactions of GBNs with plasma proteins and blood cells, including erythrocytes [200,216]. The effect of the blood protein corona in reducing the strong size-dependent hemolysis induced by pristine GO was demonstrated by Papi et al. [217].

Several functionalization strategies based on covalent and non-covalent immobilization techniques have been investigated to reduce GBN toxicity, or to improve their appropriateness for drug delivery etc., including attachment of biomolecules (e.g., proteins, lipids, mono- or poly-saccharides, etc.) and functional groups. Carboxylated GO-lanthanum complexes have shown <5% hemolysis [218], while mannosylation of GO decreased the amount of proteins in the hard corona and contributed to about a 75% reduction of GO-induced hemolysis, as possibly related to a decrease of electrostatic charges on mannosylated-GO respect to pristine GO [219]. An increased degree of graphene surface fluorination [220] or COOH⁺-implantation [221] was found to reduce considerably the adhesion and aggregation of platelets, while maintaining low hemolysis levels comparable to pristine graphene. Based on different *in vivo* studies, dextran-coated GO had maximum tolerable dose between 50 mg/kg and 125 mg/kg, with a blood half-life <30 min, with no effects in the cardiovascular parameters or hematological factors, including total hemoglobin concentration at doses <125 mg/kg [222]. When testing the hemotoxicity of GO nanostructures functionalized with arginine, lysine, and ginsenoside Rh2, Zare-Zardini and colleagues found that pristine GO had the highest values of hemolysis (50% hemolysis at 250 µg/mL particle concentration), while Rh2-functionalized GO showed the lowest hemolysis activity and the lowest effect on the intrinsic and extrinsic coagulation systems [223].

A very broad panorama emerges when exploring the interactions of graphene and its derivatives with blood components. An updated review of the literature shows that several factors may be involved, including GBN size, zeta potential, concentration, dispersion and degree of reduction of GO and rGO sheets [198], surface functionalization, as well as environmental conditions [195]. All these

factors should be considered and appropriately tuned to direct the host response to graphene-based nanostructures towards the desired hemocompatibility.

8. Comparative Analysis

On the whole, numerous studies considering the interactions of CNTs and GBNs with blood and its components have been proposed in the literature, while less extensive investigations have been conducted on NDs, CDs and fullerenes, and only few comparative analyses have examined the hemocompatibility of different types of CNs simultaneously. For instance, CNTs and GBNs have been compared, since CNTs can be seen as rolled-up graphene sheets, and the effect of surface curvature on protein binding has been evaluated. Although several discordant theories have been proposed, the most accredited ones, based on both simulations and experimental analysis, indicate a higher protein absorption as the surface curvature of the CNs decreases, with a dramatic enhancement in protein adsorption capacity on 2-D CNs compared to 1-D CNs. [140,142,200,224]. Studying protein adsorption from human serum on three different CNs, including carbon black, MWCNTs, and GO [142], Sopotnik et al. found that MWCNTs had a significantly higher affinity for HSA respect to GO but GO absorbed serum proteins other than albumin in greater amount and in a wider spectrum. The authors also showed that when the different CNs were incubated with cholinesterases, the lowest adsorption and enzyme inhibition occurred with MWCNTs, as possible consequence of a higher surface curvature respect to GO. Another recent study analyzed the interaction of three major blood proteins (i.e., HSA, human γ -globulin, and Fng) with different carbon nanomaterials, namely carbon nanotubes (COOH-MWCNTs), graphene nanoplatelets (GNPs), and porous graphene oxide (PGO) [224], showing that the formation of nanomaterial-protein complexes took place with different loading capacity depending on the protein type. Albumin was preferentially adsorbed onto GNPs, followed by COOH-MWCNTs and PGO, while γ -globulin and large Fng molecules were adsorbed with highest loading capacity on PGO, which presented high surface area and higher density of oxygenated functional groups. The presence of oxygen-based surface functional groups also influenced the fluorescence quenching efficiency, which was higher for CNTs than for GNPs. In agreement with other authors [225–227], Kenry and colleagues concluded that the influence of CNs on plasma components is protein-specific and depends on several characteristics of the nanomaterials, such as abundance of oxygenated functional groups (e.g., C-O and C=O), surface curvature, and surface area [224].

Regarding the interaction with platelets, SWCNTs and MWCNTs at the concentration 100 $\mu\text{g/mL}$ showed high platelet aggregating activity (>25%), while C60 fullerene (nC60) and fullerenol (C60(OH)24) did not present any significant platelet aggregation [164]. Additionally, a study focused on the hemocompatibility of oxidized NDs for biomedical applications showed that NDs have significantly better hemocompatibility if compared to GO both in terms of hemolytic activity and coagulation response [83].

With the information available so far, it is hard to compile a hemocompatibility ranking of CNs. Table 1 attempts to summarize the current knowledge on the response of different carbon-based nanostructures to blood components and to facilitate the comparison of the different classes of CNs considered in this manuscript.

Table 1. Main outcomes of hemocompatibility studies for different classes of CNs.

CNs	Functionalization	PLATELETS	COAGULATION System	COMPLEMENT System	RBCs	In Vivo
NDs	-COOH	Activation and prothrombotic morphological alterations [82]	No effect on the intrinsic pathway (normal aPTT) [81,83]	C1q binding causes ND agglutination, phagocytosis and cytokine production [228]	Negligible hemolysis [83,84,86]. Hemolysis [85]. Erythrocyte deformation and aggregation [86]	Extensive thromboembolism in mice pulmonary vessels [82]. Absence of induced immune response [87] and inflammation [83] in mice. Well-tolerated in non-human primates and rats [88]
CFs	various	Minimal aggregation [164]. No aggregation [99]	Inhibition of fibrin polymerization [99]	-	Interaction [102,104,105] and modification of RBC membrane [101,103]. Hemolysis [103,106]	No significant effect on the development of rat carotid thrombosis [160]. Anticoagulant effects: increased tail bleeding time and inhibited thrombosis in rats [99]. Accelerated fibrinolysis [100]
CDs	various	Dose-dependent activation (P-selectin expression) [116]	Increased aPTT and PT at 1 mg/mL and 2 mg/mL [116]	Activation (increased C3a levels in blood plasma) at CD concentration ≥ 5 mg/mL [116]	Membrane deformation and hemolysis at concentrations ≥ 1 mg/mL [116]. Negligible hemolytic activity [118,119]	-
SW CNTs	Pristine	Activation and formation of platelet–granulocyte complexes [162,167]. Aggregation and activation [160]	-	Activation through classical pathway (C1q binding) [145]	No internalization, no toxicity [172]. Shape modification, fusion and hemolysis from bundled SWCNTs [175]	Accelerated thrombus formation in the microcirculation [162,163]. Amplification of vascular thrombosis in rats (carotid artery) [160]
	-COOH	Activation and formation of platelet–granulocyte complexes [167]	Activation of the contact pathway [159]	-	Dose- and time-dependent hemolysis [173]	Toxic effect on erythrocytes and transient anemia in mice [173]
MW CNTs	Pristine	Aggregation, activation [160,165] and formation of PMPs [164]. Minimal activation [158]	Activation of the intrinsic pathway [158]	Activation through classical and alternative pathway [145]. Binding of C1q and C1s-C1r-C1r-C1s but no C1q activation [153]. Consumption of C3 and C5 [154]	No significant hemolytic activity [171]	Pro-coagulant activity in a mouse model, formation of large intravascular aggregates [158]. Amplification of vascular thrombosis in rats (carotid artery) [160]

Table 1. Cont.

CNs	Functionalization	PLATELETS	COAGULATION System	COMPLEMENT System	RBCs	In Vivo
	-COOH	Minimal activation [158]. Aggregation and release of PMPs [131]. Dose-dependent activation [166]	High activation of the intrinsic pathway [158]. Reduced fibrin clot formation times [166]	Activation through classical and alternative pathway (C1, C4a, C4b adsorption) [141]	-	Little pro-coagulant effect in mice [158]
	-NH ₂	High activation and aggregation [158]. Dose-dependent activation [166]	Activation of the intrinsic pathway [158]. Reduced fibrin clot formation times [166]	Activation through classical and alternative pathway (C1, C4a, C4b adsorption) [141]	-	Modest effects on coagulation in mice—transient PLT depletion [158]
GBNs	Pristine	Absence of activation and aggregation [210]	Normal values of PPT and aPTT [210]	-	No hemolytic effect up to 75 µg/mL [210] Hemolysis GS < GO [213]	-
GO	Variable content of oxygen-based groups	Strong aggregation and slight activation (GO > rGO) [211]	Prolonged aPTT [83]	Activation (increase of SC5b-9 and C4d levels) proportional to oxygen surface content [205]	Dose-dependent hemolytic activity [212,213]. Change of cell morphology and hemoglobin release [83]	Extensive pulmonary thromboembolism in mice [211]. Pathological effects when administered intravenously in mice [212]

According to the data available so far, biological responses at different levels can be triggered by blood exposure of different types of CNs. Most CNs induce some kind of activation, with critical outcomes in particular for CNTs. Basic surface modifications, including for example carboxyl or amine functional groups, did not induce considerable improvements of hemocompatibility. 0-D nanostructures, such as NDs and CFs, exhibited some promising results, with a high level of toleration and absence of adverse thrombotic events in most of the *in vivo* studies performed so far. As for CDs, further investigations are needed to better define the hemocompatibility of this new class of CNs that includes a wide range of nanoparticles that can be synthesis with several different approaches. Relatively good performances in terms of blood compatibility have been reported for graphene, possibly related to its ability to bind plasma proteins through stable hydrophobic interactions and π - π stacking. However, pristine graphene is unlikely to be used in biomedicine since it is hydrophobic and poorly dispersible in organic fluids. On the other hand, the more easily dispersible and functionalizable GO hydrophilic sheets present more challenging interactions with blood, and can induce increasing adverse events, such as hemolysis, PLT and complement activation, with increasing nanoparticle concentration and surface oxygen content.

To date, the state of the art does not provide definitive answers to the complex question of CN hemocompatibility. Several issues still need to be addresses (see empty boxes in Table 1), and contradictory results must be better clarified. Research should now be directed to expand the knowledge of CN hemocompatibility with a global approach and, on the other hand, to look for surface modifications that can improve the hemocompatibility of the various types of CNs and expand their functionality while preserving their specific key characteristics.

9. Conclusions

Among the various types of nanoparticles recently discovered, nanosized carbon allotropes have gained significant consideration in the biomedical field thanks to their ground-breaking characteristics (optical, electrical, mechanical, etc.) associated with versatility and ease of production and functionalization. Hemocompatibility is a major concern for nanomedicine since the use of nanostructures for diagnostic, therapeutic and regenerative medicine purposes is restricted to the absence of adverse events following injection into the blood stream.

This review summarizes the state-of-the-art of the phenomena taking place at the molecular and cellular level when CNs are exposed to blood, including plasma protein adsorption, platelet activation/aggregation, thrombus formation, activation of complement and leukocytes, and hemolysis. Different types of CNs have been considered in detail, including nanodiamonds, fullerenes, carbon dots, carbon nanotubes, and graphene. Although they are all carbon-based structures, many factors differentiate them and influence their interaction with blood components. Physicochemical properties, such as shape, curvature, surface energy, local charge, crystallinity, and hydration, play a key role in guiding protein adsorption phenomena at the blood–CN interface and the composition and conformation of the protein corona can, in turn, contribute to modulate the overall hemocompatibility response. If different types of CNs show different responses, even within the same class there may be discrepancies in behavior due to factors such as size, particle aggregation/dispersion degree, or presence of surface functionalization.

Significant progress has been made in recent years in the analysis of protein corona and hemocompatibility of CNs, however several studies often show discordant results, as partly due to the variability of nanoparticle production and purification methods, to the presence of contaminants or surface functionalization. This implies that the blood compatibility of CNs should be thoroughly assessed on a case-by-case basis. An in-depth knowledge of the biological events occurring as a result of CNs exposure to the blood environment, as well as possible strategies to improve CN hemocompatibility are fundamental for the development of advanced diagnostic and therapeutic systems based on carbon nanostructures.

Funding: This research received no external funding.

Acknowledgments: M.F. would like to thank Giorgio Speranza and Laszlo Sajti for useful discussions and comments on the manuscript.

Conflicts of Interest: The authors declare no conflict of interest.

References

1. Georgakilas, V.; Perman, J.A.; Tucek, J.; Zboril, R. Broad Family of Carbon Nanoallotropes: Classification, Chemistry, and Applications of Fullerenes, Carbon Dots, Nanotubes, Graphene, Nanodiamonds, and Combined Superstructures. *Chem. Rev.* **2015**, *115*, 4744–4822. [[CrossRef](#)]
2. Yang, N.; Jiang, X.; Pang, D.-W. Carbon Nanostructures. In *Carbon Nanoparticles and Nanostructures*; Yang, N., Jiang, X., Pang, D.-W., Eds.; Springer International Publishing: Cham, Switzerland, 2016; ISBN 978-3-319-28780-5.
3. Notarianni, M.; Liu, J.; Vernon, K.; Motta, N. Synthesis and applications of carbon nanomaterials for energy generation and storage. *Beilstein J. Nanotechnol.* **2016**, *7*, 149–196. [[CrossRef](#)] [[PubMed](#)]
4. Knupfer, M. Electronic properties of carbon nanostructures. *Surf. Sci. Rep.* **2001**, *42*, 1–74. [[CrossRef](#)]
5. Saba, N.; Jawaid, M.; Fouad, H.; Alothman, O.Y. Nanocarbon: Preparation, properties, and applications. In *Nanocarbon and its Composites*; Elsevier: Duxford, UK, 2019; pp. 327–354.
6. Panwar, N.; Soehartono, A.M.; Chan, K.K.; Zeng, S.; Xu, G.; Qu, J.; Coquet, P.; Yong, K.-T.; Chen, X. Nanocarbons for Biology and Medicine: Sensing, Imaging, and Drug Delivery. *Chem. Rev.* **2019**, *119*, 9559–9656. [[CrossRef](#)] [[PubMed](#)]
7. Tinwala, H.; Wairkar, S. Production, surface modification and biomedical applications of nanodiamonds: A sparkling tool for theranostics. *Mater. Sci. Eng. C* **2019**, *97*, 913–931. [[CrossRef](#)]
8. Sireesha, M.; Jagadeesh Babu, V.; Kranthi Kiran, A.S.; Ramakrishna, S. A review on carbon nanotubes in biosensor devices and their applications in medicine. *Nanocomposites* **2018**, *4*, 36–57. [[CrossRef](#)]
9. Luo, P.G.; Sahu, S.; Yang, S.T.; Sonkar, S.K.; Wang, J.; Wang, H.; Lecroy, G.E.; Cao, L.; Sun, Y.P. Carbon “quantum” dots for optical bioimaging. *J. Mater. Chem. B* **2013**, *1*, 2116–2127. [[CrossRef](#)]
10. Hola, K.; Zhang, Y.; Wang, Y.; Giannelis, E.P.; Zboril, R.; Rogach, A.L. Carbon dots - Emerging light emitters for bioimaging, cancer therapy and optoelectronics. *Nano Today* **2014**, *9*, 590–603. [[CrossRef](#)]
11. Scaffaro, R.; Maio, A.; Lopresti, F.; Botta, L. Nanocarbons in Electrospun Polymeric Nanomats for Tissue Engineering: A Review. *Polymers (Basel)* **2017**, *9*, 76. [[CrossRef](#)]
12. Wang, W.; Zhu, Y.; Watari, F.; Liao, S.; Yokoyama, A.; Omori, M.; Ai, H.; Cui, F. Carbon nanotubes/hydroxyapatite nanocomposites fabricated by spark plasma sintering for bonegraft applications. *Appl. Surf. Sci.* **2012**, *262*, 194–199. [[CrossRef](#)]
13. Shi, X.; Hudson, J.L.; Spicer, P.P.; Tour, J.M.; Krishnamoorti, R.; Mikos, A.G. Injectable Nanocomposites of Single-Walled Carbon Nanotubes and Biodegradable Polymers for Bone Tissue Engineering. *Biomacromolecules* **2006**, *7*, 2237–2242. [[CrossRef](#)] [[PubMed](#)]
14. Mengesha, A.E.; Youan, B.-B.C. Nanodiamonds for drug delivery systems. *Diamond Based Mater. Biomed. Appl.* **2013**, 186–205.
15. Zhang, X.-Q.; Lam, R.; Xu, X.; Chow, E.K.; Kim, H.-J.; Ho, D. Multimodal Nanodiamond Drug Delivery Carriers for Selective Targeting, Imaging, and Enhanced Chemotherapeutic Efficacy. *Adv. Mater.* **2011**, *23*, 4770–4775. [[CrossRef](#)] [[PubMed](#)]
16. Montellano, A.; Da Ros, T.; Bianco, A.; Prato, M. Fullerene C60 as a multifunctional system for drug and gene delivery. *Nanoscale* **2011**, *3*, 4035. [[CrossRef](#)] [[PubMed](#)]
17. Tao, H.; Yang, K.; Ma, Z.; Wan, J.; Zhang, Y.; Kang, Z.; Liu, Z. In vivo NIR fluorescence imaging, biodistribution, and toxicology of photoluminescent carbon dots produced from carbon nanotubes and graphite. *Small* **2012**, *8*, 281–290. [[CrossRef](#)] [[PubMed](#)]
18. Roy, U.; Drozd, V.; Durygin, A.; Rodriguez, J.; Barber, P.; Atluri, V.; Liu, X.; Voss, T.G.; Saxena, S.; Nair, M. Characterization of Nanodiamond-based anti-HIV drug Delivery to the Brain. *Sci. Rep.* **2018**, *8*, 1603. [[CrossRef](#)]
19. Liu, K.-K.; Zheng, W.-W.; Wang, C.-C.; Chiu, Y.-C.; Cheng, C.-L.; Lo, Y.-S.; Chen, C.; Chao, J.-I. Covalent linkage of nanodiamond-paclitaxel for drug delivery and cancer therapy. *Nanotechnology* **2010**, *21*, 315106. [[CrossRef](#)]

20. Li, J.; Zhu, Y.; Li, W.; Zhang, X.; Peng, Y.; Huang, Q. Nanodiamonds as intracellular transporters of chemotherapeutic drug. *Biomaterials* **2010**, *31*, 8410–8418. [[CrossRef](#)]
21. Periasamy, V.S.; Athinarayanan, J.; Alfawaz, M.A.; Alshatwi, A.A. Carbon nanoparticle induced cytotoxicity in human mesenchymal stem cells through upregulation of TNF3, NFKBIA and BCL2L1 genes. *Chemosphere* **2016**, *144*, 275–284. [[CrossRef](#)]
22. Kurantowicz, N.; Sawosz, E.; Halik, G.; Strojny, B.; Hotowy, A.; Grodzik, M.; Piast, R.; Pasanphan, W.; Chwalibog, A. Toxicity studies of six types of carbon nanoparticles in a chicken-embryo model. *Int. J. Nanomed.* **2017**, *12*, 2887–2898. [[CrossRef](#)]
23. Madannejad, R.; Shoaie, N.; Jahanpeyma, F.; Darvishi, M.H.; Azimzadeh, M.; Javadi, H. Toxicity of carbon-based nanomaterials: Reviewing recent reports in medical and biological systems. *Chem. Biol. Interact.* **2019**, *307*, 206–222. [[CrossRef](#)]
24. Kolosnjaj, J.; Szwarc, H.; Moussa, F. Toxicity Studies of Fullerenes and Derivatives. In *Advances in Experimental Medicine and Biology*; Springer: New York, NY, USA, 2007; Volume 620, pp. 168–180. ISBN 9780387767123.
25. Jia, G.; Wang, H.; Yan, L.; Wang, X.; Pei, R.; Yan, T.; Zhao, Y.; Guo, X. Cytotoxicity of carbon nanomaterials: Single-wall nanotube, multi-wall nanotube, and fullerene. *Environ. Sci. Technol.* **2005**, *39*, 1378–1383. [[CrossRef](#)]
26. Schrand, A.M.; Dai, L.; Schlager, J.J.; Hussain, S.M.; Osawa, E. Differential biocompatibility of carbon nanotubes and nanodiamonds. *Diam. Relat. Mater.* **2007**, *16*, 2118–2123. [[CrossRef](#)]
27. Fisher, C.; Rider, A.E.; Jun Han, Z.; Kumar, S.; Levchenko, I.; Ostrikov, K. Applications and nanotoxicity of carbon nanotubes and graphene in biomedicine. *J. Nanomater.* **2012**, *2012*. [[CrossRef](#)]
28. Lanone, S.; Andujar, P.; Kermanizadeh, A.; Boczkowski, J. Determinants of carbon nanotube toxicity. *Adv. Drug Deliv. Rev.* **2013**, *65*, 2063–2069. [[CrossRef](#)]
29. Johnston, H.J.; Hutchison, G.R.; Christensen, F.M.; Aschberger, K.; Stone, V. The biological mechanisms and physicochemical characteristics responsible for driving fullerene toxicity. *Toxicol. Sci.* **2009**, *114*, 162–182. [[CrossRef](#)]
30. Yan, L.; Zhao, F.; Li, S.; Hu, Z.; Zhao, Y. Low-toxic and safe nanomaterials by surface-chemical design, carbon nanotubes, fullerenes, metallofullerenes, and graphenes. *Nanoscale* **2011**, *3*, 362–382. [[CrossRef](#)]
31. Adach, K.; Fijalkowski, M.; Gajek, G.; Skolimowski, J.; Kontek, R.; Blaszczyk, A. Studies on the cytotoxicity of diamond nanoparticles against human cancer cells and lymphocytes. *Chem. Biol. Interact.* **2016**, *254*, 156–166. [[CrossRef](#)]
32. Dönmez Güngüneş, Ç.; Şeker, Ş.; Elçin, A.E.; Elçin, Y.M. A comparative study on the in vitro cytotoxic responses of two mammalian cell types to fullerenes, carbon nanotubes and iron oxide nanoparticles. *Drug Chem. Toxicol.* **2017**, *40*, 215–227. [[CrossRef](#)]
33. Yuan, X.; Zhang, X.; Sun, L.; Wei, Y.; Wei, X. Cellular Toxicity and Immunological Effects of Carbon-based Nanomaterials. *Part. Fibre Toxicol.* **2019**, *16*, 18. [[CrossRef](#)]
34. Rahmati, M.; Mozafari, M. Biological response to carbon-family nanomaterials: Interactions at the nano-bio interface. *Front. Bioeng. Biotechnol.* **2019**, *7*, 1–22. [[CrossRef](#)]
35. Uo, M.; Akasaka, T.; Watari, F.; Sato, Y.; Tohji, K. Toxicity evaluations of various carbon nanomaterials. *Dent. Mater. J.* **2011**, *30*, 245–263. [[CrossRef](#)]
36. Bhattacharya, K.; Mukherjee, S.P.; Gallud, A.; Burkert, S.C.; Bistarelli, S.; Bellucci, S.; Bottini, M.; Star, A.; Fadeel, B. Biological interactions of carbon-based nanomaterials: From coronation to degradation. *Nanomed. Nanotechnol. Biol. Med.* **2016**, *12*, 333–351. [[CrossRef](#)]
37. Vroman, L. When Blood Is Touched. *Materials (Basel)* **2009**, *2*, 1547–1557. [[CrossRef](#)]
38. Brash, J.L. Studies of protein adsorption relevant to blood compatible materials. In *Modern Aspects of Protein Adsorption on Biomaterials*; Springer: Dordrecht, The Netherlands, 1991; pp. 39–47.
39. Horbett, T.A. Protein Adsorption on Biomaterials. In *Biomaterials: Interfacial Phenomena and Applications*; American Chemical Society: Washington, DC, USA, 1982; pp. 233–244.
40. Vroman, L.; Adams, A.L.; Fischer, G.C.; Munoz, P.C. Interaction of high molecular weight kininogen, factor XII, and fibrinogen in plasma at interfaces. *Blood* **1980**, *55*, 156–159. [[CrossRef](#)]
41. Anderson, N.L.; Anderson, N.G. The human plasma proteome: History, character, and diagnostic prospects. *Mol. Cell. Proteomics* **2002**, *1*, 845–867. [[CrossRef](#)]
42. Andrade, J.; Hlady, V. Plasma Protein Adsorption: The Big Twelve. *Ann. N. Y. Acad. Sci.* **1987**, *516*, 158–172. [[CrossRef](#)]

43. Hoffman, A.S. Blood—Biomaterial Interactions: An Overview. In *Biomaterials: Interfacial Phenomena and Applications*; Cooper, Ed.; American Chemical Society: Washington, DC, USA, 1982; pp. 3–8.
44. Jaffer, I.H.; Fredenburgh, J.C.; Hirsh, J.; Weitz, J.I. Medical device-induced thrombosis: What causes it and how can we prevent it? *J. Thromb. Haemost.* **2015**, *13*, S72–S81. [[CrossRef](#)]
45. Tsai, W.-B.; Grunkemeier, J.M.; Horbett, T.A. Human plasma fibrinogen adsorption and platelet adhesion to polystyrene. *J. Biomed. Mater. Res.* **1999**, *44*, 130–139. [[CrossRef](#)]
46. Tzoneva, R.; Heuchel, M.; Groth, T.; Altankov, G.; Albrecht, W.; Paul, D. Fibrinogen adsorption and platelet interactions on polymer membranes. *J. Biomater. Sci. Polym. Ed.* **2002**, *13*, 1033–1050. [[CrossRef](#)]
47. Yan, Y.; Xu, L.C.; Vogler, E.A.; Siedlecki, C.A. Contact activation by the intrinsic pathway of blood plasma coagulation. In *Hemocompatibility of Biomaterials for Clinical Applications: Blood-Biomaterials Interactions*; Elsevier Inc.: Duxford, UK, 2018; pp. 3–28, ISBN 9780081004999.
48. Nilsson, B.; Ekdahl, K.N.; Mollnes, T.E.; Lambris, J.D. The role of complement in biomaterial-induced inflammation. *Mol. Immunol.* **2007**, *44*, 82–94. [[CrossRef](#)]
49. Vogler, E.A.; Siedlecki, C.A. Contact activation of blood-plasma coagulation. *Biomaterials* **2009**, *30*, 1857–1869. [[CrossRef](#)]
50. Engberg, A.E.; Rosengren-Holmberg, J.P.; Chen, H.; Nilsson, B.; Lambris, J.D.; Nicholls, I.A.; Ekdahl, K.N. Blood protein-polymer adsorption: Implications for understanding complement-mediated hemoincompatibility. *J. Biomed. Mater. Res. Part A* **2011**, *97A*, 74–84. [[CrossRef](#)]
51. Mödinger, Y.; Teixeira, G.Q.; Neidlinger-Wilke, C.; Ignatius, A. Role of the Complement System in the Response to Orthopedic Biomaterials. *Int. J. Mol. Sci.* **2018**, *19*, 3367. [[CrossRef](#)]
52. Ekdahl, K.N.; Lambris, J.D.; Elwing, H.; Ricklin, D.; Nilsson, P.H.; Teramura, Y.; Nicholls, I.A.; Nilsson, B. Innate immunity activation on biomaterial surfaces: A Mechanistic Model and Coping Strategies. *Adv. Drug Deliv. Rev.* **2012**, *63*, 1042–1050. [[CrossRef](#)]
53. Andersson, J.; Ekdahl, K.N.; Larsson, R.; Nilsson, U.R.; Nilsson, B. C3 Adsorbed to a Polymer Surface Can Form an Initiating Alternative Pathway Convertase. *J. Immunol.* **2002**, *168*, 5786–5791. [[CrossRef](#)]
54. Weber, M.; Steinle, H.; Golombek, S.; Hann, L.; Schlensak, C.; Wendel, H.P.; Avci-Adali, M. Blood-Contacting Biomaterials: In Vitro Evaluation of the Hemocompatibility. *Front. Bioeng. Biotechnol.* **2018**, *6*, 99. [[CrossRef](#)]
55. Gorbet, M.B.; Sefton, M. V Biomaterial-associated thrombosis: Roles of coagulation factors, complement, platelets and leukocytes. *Biomaterials* **2004**, *25*, 5681–5703. [[CrossRef](#)]
56. Nel, A.E.; Mädler, L.; Velegol, D.; Xia, T.; Hoek, E.M.V.; Somasundaran, P.; Klaessig, F.; Castranova, V.; Thompson, M. Understanding biophysicochemical interactions at the nano-bio interface. *Nat. Mater.* **2009**, *8*, 543–557. [[CrossRef](#)]
57. Cedervall, T.; Lynch, I.; Lindman, S.; Berggård, T.; Thulin, E.; Nilsson, H.; Dawson, K.A.; Linse, S. Understanding the nanoparticle-protein corona using methods to quantify exchange rates and affinities of proteins for nanoparticles. *Proc. Natl. Acad. Sci. USA* **2007**, *104*, 2050–2055. [[CrossRef](#)]
58. Lundqvist, M.; Augustsson, C.; Lilja, M.; Lundkvist, K.; Dahlbäck, B.; Linse, S.; Cedervall, T. The nanoparticle protein corona formed in human blood or human blood fractions. *PLoS ONE* **2017**, *12*, e0175871. [[CrossRef](#)] [[PubMed](#)]
59. Monopoli, M.P.; Åberg, C.; Salvati, A.; Dawson, K.A. Biomolecular coronas provide the biological identity of nanosized materials. *Nat. Nanotechnol.* **2012**, *7*, 779–786. [[CrossRef](#)] [[PubMed](#)]
60. Walkey, C.D.; Chan, W.C.W. Understanding and controlling the interaction of nanomaterials with proteins in a physiological environment. *Chem. Soc. Rev.* **2012**, *41*, 2780–2799. [[CrossRef](#)] [[PubMed](#)]
61. Wolfram, J.; Yang, Y.; Shen, J.; Moten, A.; Chen, C.; Shen, H.; Ferrari, M.; Zhao, Y. The nano-plasma interface: Implications of the protein corona. *Colloids Surfaces B Biointerfaces* **2014**, *124*, 17–24. [[CrossRef](#)] [[PubMed](#)]
62. Loh, K.P.; Lim, C.T. Molecular interactions of graphene oxide with human blood plasma proteins. *Nanoscale* **2016**, *8*, 9425–9441.
63. Cai, R.; Chen, C. The Crown and the Scepter: Roles of the Protein Corona in Nanomedicine. *Adv. Mater.* **2018**, *1805740*, 1–13. [[CrossRef](#)]
64. Saha, K.; Moyano, D.F.; Rotello, V.M. Protein coronas suppress the hemolytic activity of hydrophilic and hydrophobic nanoparticles. *Mater. Horizons* **2014**, *1*, 102–105. [[CrossRef](#)]
65. Ge, C.; Tian, J.; Zhao, Y.; Chen, C.; Zhou, R.; Chai, Z. Towards understanding of nanoparticle–protein corona. *Arch. Toxicol.* **2015**, *89*, 519–539. [[CrossRef](#)]

66. Nienhaus, K.; Nienhaus, G.U. Towards a molecular-level understanding of the protein corona around nanoparticles—Recent advances and persisting challenges. *Curr. Opin. Biomed. Eng.* **2019**, *10*, 11–22. [[CrossRef](#)]
67. Schrand, A.M.; Hens, S.A.C.; Shenderova, O.A. Nanodiamond Particles: Properties and Perspectives for Bioapplications. *Crit. Rev. Solid State Mater. Sci.* **2009**, *34*, 18–74. [[CrossRef](#)]
68. Hanada, K. Detonation nanodiamond: Perspective and Applications. *Surf. Eng.* **2009**, *25*, 487–489. [[CrossRef](#)]
69. Mochalin, V.N.; Shenderova, O.; Ho, D.; Gogotsi, Y. The properties and applications of nanodiamonds. *Nat. Nanotechnol.* **2012**, *7*, 11–23. [[CrossRef](#)] [[PubMed](#)]
70. Vijayanthimala, V.; Lee, D.K.; Kim, S.V.; Yen, A.; Tsai, N.; Ho, D.; Chang, H.-C.; Shenderova, O. Nanodiamond-mediated drug delivery and imaging: Challenges and opportunities. *Expert Opin. Drug Deliv.* **2015**, *12*, 735–749. [[CrossRef](#)] [[PubMed](#)]
71. Chen, M.; Pierstorff, E.D.; Lam, R.; Li, S.-Y.; Huang, H.; Osawa, E.; Ho, D. Nanodiamond-Mediated Delivery of Water-Insoluble Therapeutics. *ACS Nano* **2009**, *3*, 2016–2022. [[CrossRef](#)] [[PubMed](#)]
72. Xing, Z.; Pedersen, T.O.; Wu, X.; Xue, Y.; Sun, Y.; Finne-Wistrand, A.; Kloss, F.R.; Waag, T.; Krueger, A.; Steinmüller-Nethl, D.; et al. Biological Effects of Functionalizing Copolymer Scaffolds with Nanodiamond Particles. *Tissue Eng. Part A* **2013**, *19*, 1783–1791. [[CrossRef](#)] [[PubMed](#)]
73. Hopper, A.P.; Dugan, J.M.; Gill, A.A.; Fox, O.J.L.; May, P.W.; Haycock, J.W.; Claeysens, F. Amine functionalized nanodiamond promotes cellular adhesion, proliferation and neurite outgrowth. *Biomed. Mater.* **2014**, *9*, 045009. [[CrossRef](#)]
74. Whitlow, J.; Pacelli, S.; Paul, A. Multifunctional nanodiamonds in regenerative medicine: Recent advances and future directions. *J. Control. Release* **2017**, *261*, 62–86. [[CrossRef](#)]
75. Keremidarska, M.; Ganeva, A.; Mitev, D.; Hikov, T.; Presker, R.; Pramatarova, L.; Krasteva, N. Comparative study of cytotoxicity of detonation nanodiamond particles with an osteosarcoma cell line and primary mesenchymal stem cells. *Biotechnol. Biotechnol. Equip.* **2014**, *28*, 733–739. [[CrossRef](#)]
76. Paget, V.; Sergent, J.A.; Grall, R.; Altmeyer-Morel, S.; Girard, H.A.; Petit, T.; Gesset, C.; Mermoux, M.; Bergonzo, P.; Arnault, J.C.; et al. Carboxylated nanodiamonds are neither cytotoxic nor genotoxic on liver, kidney, intestine and lung human cell lines. *Nanotoxicology* **2014**, *8*, 46–56. [[CrossRef](#)]
77. Chang, H.-C.; Hsiao, W.W.-W.; Su, M.-C. Biocompatibility of Nanodiamonds. In *Fluorescent Nanodiamonds*; John Wiley & Sons, Ltd.: Chichester, UK, 2018; pp. 73–89.
78. Lin, C.-L.; Lin, C.-H.; Chang, H.-C.; Su, M.-C. Protein Attachment on Nanodiamonds. *J. Phys. Chem. A* **2015**, *119*, 7704–7711. [[CrossRef](#)]
79. Aramesh, M.; Shimoni, O.; Ostrikov, K.; Praver, S.; Cervenka, J. Surface charge effects in protein adsorption on nanodiamonds. *Nanoscale* **2015**, *7*, 5726–5736. [[CrossRef](#)] [[PubMed](#)]
80. Wang, H.D.; Niu, C.H.; Yang, Q.; Badea, I. Study on protein conformation and adsorption behaviors in nanodiamond particle-protein complexes. *Nanotechnology* **2011**, *22*, 145703. [[CrossRef](#)] [[PubMed](#)]
81. Mona, J.; Kuo, C.J.; Perevedentseva, E.; Priezzhev, A.V.; Cheng, C.L. Adsorption of human blood plasma on nanodiamond and its influence on activated partial thromboplastin time. *Diam. Relat. Mater.* **2013**, *39*, 73–77. [[CrossRef](#)]
82. Kumari, S.; Singh, M.K.; Singh, S.K.; Grácio, J.J.; Dash, D. Nanodiamonds activate blood platelets and induce thromboembolism. *Nanomedicine* **2014**, *9*, 427–440. [[CrossRef](#)] [[PubMed](#)]
83. Li, H.C.; Hsieh, F.J.; Chen, C.P.; Chang, M.Y.; Hsieh, P.C.H.; Chen, C.C.; Hung, S.U.; Wu, C.C.; Chang, H.C. The hemocompatibility of oxidized diamond nanocrystals for biomedical applications. *Sci. Rep.* **2013**, *3*, 1–8. [[CrossRef](#)] [[PubMed](#)]
84. Wasowicz, M.; Ficek, M.; Wróbel, M.S.; Chakraborty, R.; Fixler, D.; Wierzbna, P.; Jędrzejewska-Szczerska, M. Haemocompatibility of modified nanodiamonds. *Materials (Basel)* **2017**, *10*, 352. [[CrossRef](#)]
85. Puzyr, A.P.; Neshumaev, D.A.; Tarskikh, S.V.; Makarskaya, G.V.; Dolmatov, V.Y.; Bondar, V.S. Destruction of human blood cells in interaction with detonation nanodiamonds in experiments in vitro. *Diam. Relat. Mater.* **2004**, *13*, 2020–2023. [[CrossRef](#)]
86. Lin, Y.-C. The influence of nanodiamond on the oxygenation states and micro rheological properties of human red blood cells in vitro. *J. Biomed. Opt.* **2012**, *17*, 101512. [[CrossRef](#)]
87. Tsai, L.W.; Lin, Y.C.; Perevedentseva, E.; Lugovtsov, A.; Priezzhev, A.; Cheng, C.L. Nanodiamonds for medical applications: Interaction with blood in vitro and in vivo. *Int. J. Mol. Sci.* **2016**, *17*, 5. [[CrossRef](#)]

88. Moore, L.; Yang, J.; Lan, T.T.H.; Osawa, E.; Lee, D.K.; Johnson, W.D.; Xi, J.; Chow, E.K.H.; Ho, D. Biocompatibility Assessment of Detonation Nanodiamond in Non-Human Primates and Rats Using Histological, Hematologic, and Urine Analysis. *ACS Nano* **2016**, *10*, 7385–7400. [[CrossRef](#)]
89. Bakry, R.; Vallant, R.M.; Najam-ul-Haq, M.; Rainer, M.; Szabo, Z.; Huck, C.W.; Bonn, G.K. Medicinal applications of fullerenes. *Int. J. Nanomed.* **2007**, *2*, 639–649. [[PubMed](#)]
90. Goodarzi, S.; Da Ros, T.; Conde, J.; Sefat, F.; Mozafari, M. Fullerene: Biomedical engineers get to revisit an old friend. *Mater. Today* **2017**, *20*, 460–480. [[CrossRef](#)]
91. Castro, E.; Garcia, A.H.; Zavala, G.; Echegoyen, L. Fullerenes in biology and medicine. *J. Mater. Chem. B* **2017**, *5*, 6523–6535. [[CrossRef](#)] [[PubMed](#)]
92. Gharbi, N.; Pressac, M.; Hadchouel, M.; Szwarc, H.; Wilson, S.R.; Moussa, F. [60]Fullerene is a Powerful Antioxidant in Vivo with No Acute or Subacute Toxicity. *Nano Lett.* **2005**, *5*, 2578–2585. [[CrossRef](#)] [[PubMed](#)]
93. Nakagawa, Y.; Suzuki, T.; Ishii, H.; Nakae, D.; Ogata, A. Cytotoxic effects of hydroxylated fullerenes on isolated rat hepatocytes via mitochondrial dysfunction. *Arch. Toxicol.* **2011**, *85*, 1429–1440. [[CrossRef](#)] [[PubMed](#)]
94. Shimizu, K.; Kubota, R.; Kobayashi, N.; Tahara, M.; Sugimoto, N.; Nishimura, T.; Ikarashi, Y. Cytotoxic Effects of Hydroxylated Fullerenes in Three Types of Liver Cells. *Materials (Basel)* **2013**, *6*, 2713–2722. [[CrossRef](#)]
95. Sayes, C.M.; Fortner, J.D.; Guo, W.; Lyon, D.; Boyd, A.M.; Ausman, K.D.; Tao, Y.J.; Sitharaman, B.; Wilson, L.J.; Hughes, J.B.; et al. The Differential Cytotoxicity of Water-Soluble Fullerenes. *Nano Lett.* **2004**, *4*, 1881–1887. [[CrossRef](#)]
96. Trpkovic, A.; Todorovic-Markovic, B.; Trajkovic, V. Toxicity of pristine versus functionalized fullerenes: Mechanisms of cell damage and the role of oxidative stress. *Arch. Toxicol.* **2012**, *86*, 1809–1827. [[CrossRef](#)]
97. Yang, L.-Y.; Hua, S.-Y.; Zhou, Z.-Q.; Wang, G.-C.; Jiang, F.-L.; Liu, Y. Characterization of fullerene-protein interactions and an extended investigation on cytotoxicity. *Colloids Surf. B Biointerfaces* **2017**, *157*, 261–267. [[CrossRef](#)]
98. Deguchi, S.; Yamazaki, T.; Mukai, S.; Usami, R.; Horikoshi, K. Stabilization of C₆₀ Nanoparticles by Protein Adsorption and Its Implications for Toxicity Studies. *Chem. Res. Toxicol.* **2007**, *20*, 854–858. [[CrossRef](#)]
99. Xia, S.; Li, J.; Zu, M.; Li, J.; Liu, J.; Bai, X.; Chang, Y.; Chen, K.; Gu, W.; Zeng, L.; et al. Small size fullerene nanoparticles inhibit thrombosis and blood coagulation through inhibiting activities of thrombin and FXa. *Nanomed. Nanotechnol. Biol. Med.* **2018**, *14*, 929–939. [[CrossRef](#)] [[PubMed](#)]
100. Andrievsky, G.; Shakhnin, D.; Tronza, A.; Zhernosekov, D.; Tykhomyrov, A. The acceleration of blood plasma clot lysis in the presence of hydrated C₆₀ fullerene nanostructures in super-small concentration. *Fuller. Nanotub. Carbon Nanostruct.* **2010**, *18*, 303–311. [[CrossRef](#)]
101. Zhang, X.; Zhang, Y.; Zheng, Y.; Wang, B. Mechanical characteristics of human red blood cell membrane change due to C₆₀ nanoparticle infiltration. *Phys. Chem. Chem. Phys.* **2013**, *15*, 2473–2481. [[CrossRef](#)] [[PubMed](#)]
102. Qiao, R.; Roberts, A.P.; Mount, A.S.; Klaine, S.J.; Ke, P.C. Translocation of C₆₀ and Its Derivatives Across a Lipid Bilayer. *Nano Lett.* **2007**, *7*, 614–619. [[CrossRef](#)] [[PubMed](#)]
103. Trpkovic, A.; Todorovic-Markovic, B.; Kleut, D.; Misirkic, M.; Janjetovic, K.; Vucicevic, L.; Pantovic, A.; Jovanovic, S.; Dramicanin, M.; Markovic, Z.; et al. Oxidative stress-mediated hemolytic activity of solvent exchange-prepared fullerene (C₆₀) nanoparticles. *Nanotechnology* **2010**, *21*, 375102. [[CrossRef](#)]
104. Avilova, I.; Khakina, E.; Kraevaya, O.; Kotelnikov, A.; Kotelnikova, R.; Troshin, P.; Volkov, V. Self-diffusion of water-soluble fullerene derivatives in mouse erythrocytes. *Biochim. Biophys. Acta Biomembr.* **2018**, *1860*, 1537–1543. [[CrossRef](#)]
105. Yang, X.L.; Huang, C.; Qiao, X.G.; Yao, L.; Zhao, D.X.; Tan, X. Photo-induced lipid peroxidation of erythrocyte membranes by a bis-methanophosphonate fullerene. *Toxicol. Vitro.* **2007**, *21*, 1493–1498. [[CrossRef](#)]
106. Bosi, S.; Feruglio, L.; Da Ros, T.; Spalluto, G.; Gregoretto, B.; Terdoslavich, M.; Decorti, G.; Passamonti, S.; Moro, S.; Prato, M. Hemolytic effects of water-soluble fullerene derivatives. *J. Med. Chem.* **2004**, *47*, 6711–6715. [[CrossRef](#)]
107. Xu, X.; Ray, R.; Gu, Y.; Ploehn, H.J.; Gearheart, L.; Raker, K.; Scrivens, W.A. Electrophoretic Analysis and Purification of Fluorescent Single-Walled Carbon Nanotube Fragments. *J. Am. Chem. Soc.* **2004**, *126*, 12736–12737. [[CrossRef](#)]
108. Baker, S.N.; Baker, G.A. Luminescent carbon nanodots: Emergent nanolights. *Angew. Chemie Int. Ed.* **2010**, *49*, 6726–6744. [[CrossRef](#)]

109. Sciortino, A.; Cannizzo, A.; Messina, F. Carbon Nanodots: A Review—From the Current Understanding of the Fundamental Photophysics to the Full Control of the Optical Response. *C J. Carbon Res.* **2018**, *4*, 67. [[CrossRef](#)]
110. Yang, S.T.; Wang, X.; Wang, H.; Lu, F.; Luo, P.G.; Cao, L.; Mezziani, M.J.; Liu, J.H.; Liu, Y.; Chen, M.; et al. Carbon dots as nontoxic and high-performance fluorescence imaging agents. *J. Phys. Chem. C* **2009**, *113*, 18110–18114. [[CrossRef](#)] [[PubMed](#)]
111. Yang, S.-T.; Cao, L.; Luo, P.G.; Lu, F.; Wang, X.; Wang, H.; Mezziani, M.J.; Liu, Y.; Qi, G.; Sun, Y.-P. Carbon Dots for Optical Imaging in Vivo. *J. Am. Chem. Soc.* **2009**, *131*, 11308–11309. [[CrossRef](#)] [[PubMed](#)]
112. Wegner, K.D.; Hildebrandt, N. Quantum dots: Bright and versatile in vitro and in vivo fluorescence imaging biosensors. *Chem. Soc. Rev.* **2015**, *44*, 4792–4834. [[CrossRef](#)]
113. Liu, J.-H.; Cao, L.; LeCroy, G.E.; Wang, P.; Mezziani, M.J.; Dong, Y.; Liu, Y.; Luo, P.G.; Sun, Y.-P. Carbon “Quantum” Dots for Fluorescence Labeling of Cells. *ACS Appl. Mater. Interfaces* **2015**, *7*, 19439–19445. [[CrossRef](#)]
114. Ray, S.C.; Saha, A.; Jana, N.R.; Sarkar, R. Fluorescent Carbon Nanoparticles: Synthesis, Characterization, and Bioimaging Application. *J. Phys. Chem. C* **2009**, *113*, 18546–18551. [[CrossRef](#)]
115. Huang, S.; Yang, E.; Yao, J.; Chu, X.; Liu, Y.; Zhang, Y.; Xiao, Q. Nitrogen, Cobalt Co-doped Fluorescent Magnetic Carbon Dots as Ratiometric Fluorescent Probes for Cholesterol and Uric Acid in Human Blood Serum. *ACS Omega* **2019**, *4*, 9333–9342. [[CrossRef](#)]
116. Li, S.; Guo, Z.; Zhang, Y.; Xue, W.; Liu, Z. Blood Compatibility Evaluations of Fluorescent Carbon Dots. *ACS Appl. Mater. Interfaces* **2015**, *7*, 19153–19162. [[CrossRef](#)]
117. Li, S.; Guo, Z.; Feng, R.; Zhang, Y.; Xue, W.; Liu, Z. Hyperbranched polyglycerol conjugated fluorescent carbon dots with improved: In vitro toxicity and red blood cell compatibility for bioimaging. *RSC Adv.* **2017**, *7*, 4975–4982. [[CrossRef](#)]
118. Zhang, R.; Liu, Y.; Yu, L.; Li, Z.; Sun, S. Preparation of high-quality biocompatible carbon dots by extraction, with new thoughts on the luminescence mechanisms. *Nanotechnology* **2013**, *24*, 225601. [[CrossRef](#)]
119. Huang, G.; Chen, X.; Wang, C.; Zheng, H.; Huang, Z.; Chen, D.; Xie, H. Photoluminescent carbon dots derived from sugarcane molasses: Synthesis, properties, and applications. *RSC Adv.* **2017**, *7*, 47840–47847. [[CrossRef](#)]
120. Cao, X.; Wang, J.; Deng, W.; Chen, J.; Wang, Y.; Zhou, J.; Du, P.; Xu, W.; Wang, Q.; Wang, Q.; et al. Photoluminescent Cationic Carbon Dots as efficient Non-Viral Delivery of Plasmid SOX9 and Chondrogenesis of Fibroblasts. *Sci. Rep.* **2018**, *8*, 7057. [[CrossRef](#)] [[PubMed](#)]
121. Iijima, S.; Ichihashi, T. Single-shell carbon nanotubes of 1-nm diameter. *Nature* **1993**, *363*, 603–605. [[CrossRef](#)]
122. Iijima, S. Carbon nanotubes: Past, present, and future. *Phys. B Condens. Matter* **2002**, *323*, 1–5. [[CrossRef](#)]
123. Iijima, S. Helical microtubules of graphitic carbon. *Nature* **1991**, *354*, 56–58. [[CrossRef](#)]
124. Iannazzo, D.; Piperno, A.; Pistone, A.; Grassi, G.; Galvagno, S. Recent Advances in Carbon Nanotubes as Delivery Systems for Anticancer Drugs. *Curr. Med. Chem.* **2013**, *20*, 1333–1354. [[CrossRef](#)]
125. Hassan, H.A.F.M.; Diebold, S.S.; Smyth, L.A.; Walters, A.A.; Lombardi, G.; Al-Jamal, K.T. Application of carbon nanotubes in cancer vaccines: Achievements, challenges and chances. *J. Control. Release* **2019**, *297*, 79–90. [[CrossRef](#)]
126. Veetil, J.V.; Ye, K. Tailored carbon nanotubes for tissue engineering applications. *Biotechnol. Prog.* **2009**, *25*, 709–721. [[CrossRef](#)]
127. Madani, S.Y.; Mandel, A.; Seifalian, A.M. A concise review of carbon nanotube’s toxicology. *Nano Rev.* **2013**, *4*, 21521. [[CrossRef](#)]
128. Smart, S.K.; Cassady, A.I.; Lu, G.Q.; Martin, D.J. The biocompatibility of carbon nanotubes. *Carbon N. Y.* **2006**, *44*, 1034–1047. [[CrossRef](#)]
129. Zhang, T.; Tang, M.; Yao, Y.; Ma, Y.; Pu, Y. MWCNT interactions with protein: Surface-induced changes in protein adsorption and the impact of protein corona on cellular uptake and cytotoxicity. *Int. J. Nanomed.* **2019**, *14*, 993–1009. [[CrossRef](#)] [[PubMed](#)]
130. Marchesan, S.; Prato, M. Under the lens: Carbon nanotube and protein interaction at the nanoscale. *Chem. Commun.* **2015**, *51*, 4347–4359. [[CrossRef](#)] [[PubMed](#)]
131. De Paoli, S.H.; Diduch, L.L.; Tegegn, T.Z.; Orecna, M.; Strader, M.B.; Karnaukhova, E.; Bonevich, J.E.; Holada, K.; Simak, J. The effect of protein corona composition on the interaction of carbon nanotubes with human blood platelets. *Biomaterials* **2014**, *35*, 6182–6194. [[CrossRef](#)] [[PubMed](#)]

132. Shannahan, J.H.; Brown, J.M.; Chen, R.; Ke, P.C.; Lai, X.; Mitra, S.; Witzmann, F.A. Comparison of Nanotube-Protein Corona Composition in Cell Culture Media. *Small* **2013**, *9*, 2171–2181. [[CrossRef](#)] [[PubMed](#)]
133. Zhao, M.L.; Li, D.J.; Yuan, L.; Yue, Y.C.; Liu, H.; Sun, X. Differences in cytocompatibility and hemocompatibility between carbon nanotubes and nitrogen-doped carbon nanotubes. *Carbon N. Y.* **2011**, *49*, 3125–3133. [[CrossRef](#)]
134. Li, L.; Lin, R.; He, H.; Jiang, L.; Gao, M. Interaction of carboxylated single-walled carbon nanotubes with bovine serum albumin. *Spectrochim. Acta Part A Mol. Biomol. Spectrosc.* **2013**, *105*, 45–51. [[CrossRef](#)]
135. Lou, K.; Zhu, Z.; Zhang, H.; Wang, Y.; Wang, X.; Cao, J. Comprehensive studies on the nature of interaction between carboxylated multi-walled carbon nanotubes and bovine serum albumin. *Chem. Biol. Interact.* **2016**, *243*, 54–61. [[CrossRef](#)]
136. Guan, Y.; Zhang, H.; Wang, Y. New insight into the binding interaction of hydroxylated carbon nanotubes with bovine serum albumin. *Spectrochim. Acta Part A Mol. Biomol. Spectrosc.* **2014**, *124*, 556–563. [[CrossRef](#)]
137. Hosseinzadeh, M.; Nikjoo, S.; Zare, N.; Delavar, D.; Beigoli, S.; Chamani, J. Characterization of the structural changes of human serum albumin upon interaction with single-walled and multi-walled carbon nanotubes: Spectroscopic and molecular modeling approaches. *Res. Chem. Intermed.* **2019**, *45*, 401–423. [[CrossRef](#)]
138. Podila, R.; Vedantam, P.; Ke, P.C.; Brown, J.M.; Rao, A.M. Evidence for Charge-Transfer-Induced Conformational Changes in Carbon Nanostructure–Protein Corona. *J. Phys. Chem. C* **2012**, *116*, 22098–22103. [[CrossRef](#)]
139. Zhao, X.; Lu, D.; Hao, F.; Liu, R. Exploring the diameter and surface dependent conformational changes in carbon nanotube-protein corona and the related cytotoxicity. *J. Hazard. Mater.* **2015**, *292*, 98–107. [[CrossRef](#)] [[PubMed](#)]
140. Gu, Z.; Yang, Z.; Chong, Y.; Ge, C.; Weber, J.K.; Bell, D.R.; Zhou, R. Surface curvature relation to protein adsorption for carbon-based nanomaterials. *Sci. Rep.* **2015**, *5*, 1–9. [[CrossRef](#)] [[PubMed](#)]
141. Nicoletti, M.; Capodanno, C.; Gambarotti, C.; Fasoli, E. Proteomic investigation on bio-corona of functionalized multi-walled carbon nanotubes. *Biochim. Biophys. Acta Gen. Subj.* **2018**, *1862*, 2293–2303. [[CrossRef](#)] [[PubMed](#)]
142. Sopotnik, M.; Leonardi, A.; Križaj, I.; Dušak, P.; Makovec, D.; Mesarič, T.; Ulrih, N.P.; Junkar, I.; Sepčić, K.; Drobne, D. Comparative study of serum protein binding to three different carbon-based nanomaterials. *Carbon N. Y.* **2015**, *95*, 560–572. [[CrossRef](#)]
143. Sacchetti, C.; Motamedchaboki, K.; Magrini, A.; Palmieri, G.; Mattei, M.; Bernardini, S.; Rosato, N.; Bottini, N.; Bottini, M. Surface Polyethylene Glycol Conformation Influences the Protein Corona of Polyethylene Glycol-Modified Single-Walled Carbon Nanotubes: Potential Implications on Biological Performance. *ACS Nano* **2013**, *7*, 1974–1989. [[CrossRef](#)]
144. Morikawa, M.; Kuboki, Y.; Watari, F. Evaluation of protein adsorption to carbon nanotubes having different property, and identification of adsorbed proteins. *Nano Biomed.* **2012**, *4*, 66–75.
145. Salvador-Morales, C.; Flahaut, E.; Sim, E.; Sloan, J.; Green, M.L.H.; Sim, R.B. Complement activation and protein adsorption by carbon nanotubes. *Mol. Immunol.* **2006**, *43*, 193–201. [[CrossRef](#)]
146. Pinals, R.L.; Yang, D.; Lui, A.; Cao, W.; Landry, M.P. Corona exchange dynamics on carbon nanotubes by multiplexed fluorescence monitoring. *J. Am. Chem. Soc.* **2020**, *142*, 1254–1264. [[CrossRef](#)]
147. Dutta, D.; Sundaram, S.K.; Teeguarden, J.G.; Riley, B.J.; Fifield, L.S.; Jacobs, J.M.; Addleman, S.R.; Kaysen, G.A.; Moudgil, B.M.; Weber, T.J. Adsorbed Proteins Influence the Biological Activity and Molecular Targeting of Nanomaterials. *Toxicol. Sci.* **2007**, *100*, 303–315. [[CrossRef](#)]
148. Lu, N.; Sui, Y.; Ding, Y.; Tian, R.; Li, L.; Liu, F. Adsorption of human serum albumin on functionalized single-walled carbon nanotubes reduced cytotoxicity. *Chem. Biol. Interact.* **2018**, *295*, 64–72. [[CrossRef](#)]
149. Wang, Y.Q.; Zhang, H.M.; Cao, J. Binding of hydroxylated single-walled carbon nanotubes to two hemoproteins, hemoglobin and myoglobin. *J. Photochem. Photobiol. B Biol.* **2014**, *141*, 26–35. [[CrossRef](#)] [[PubMed](#)]
150. Ge, C.; Du, J.; Zhao, L.; Wang, L.; Liu, Y.; Li, D.; Yang, Y.; Zhou, R.; Zhao, Y.; Chai, Z.; et al. Binding of blood proteins to carbon nanotubes reduces cytotoxicity. *Proc. Natl. Acad. Sci. USA* **2011**, *108*, 16968–16973. [[CrossRef](#)] [[PubMed](#)]
151. Rybak-Smith, M.J.; Sim, R.B. Complement activation by carbon nanotubes. *Adv. Drug Deliv. Rev.* **2011**, *63*, 1031–1041. [[CrossRef](#)] [[PubMed](#)]

152. Andersen, A.J.; Wibroe, P.P.; Moghimi, S.M. Perspectives on carbon nanotube-mediated adverse immune effects. *Adv. Drug Deliv. Rev.* **2012**, *64*, 1700–1705. [[CrossRef](#)]
153. Ling, W.L.; Biro, A.; Bally, I.; Tacnet, P.; Deniaud, A.; Doris, E.; Frachet, P.; Schoehn, G.; Pebay-Peyroula, E.; Arlaud, G.J. Proteins of the Innate Immune System Crystallize on Carbon Nanotubes but Are Not Activated. *ACS Nano* **2011**, *5*, 730–737. [[CrossRef](#)]
154. Pondman, K.M.; Sobik, M.; Nayak, A.; Tsolaki, A.G.; Jäkel, A.; Flahaut, E.; Hampel, S.; ten Haken, B.; Sim, R.B.; Kishore, U. Complement activation by carbon nanotubes and its influence on the phagocytosis and cytokine response by macrophages. *Nanomed. Nanotechnol. Biol. Med.* **2014**, *10*, 1287–1299. [[CrossRef](#)]
155. Pondman, K.M.; Salvador-Morales, C.; Paudyal, B.; Sim, R.B.; Kishore, U. Interactions of the innate immune system with carbon nanotubes. *Nanoscale Horizons* **2017**, *2*, 174–186. [[CrossRef](#)]
156. Andersen, A.J.; Robinson, J.T.; Dai, H.; Hunter, A.C.; Andresen, T.L.; Moghimi, S.M. Single-Walled Carbon Nanotube Surface Control of Complement Recognition and Activation. *ACS Nano* **2013**, *7*, 1108–1119. [[CrossRef](#)]
157. Andersen, A.J.; Windschiegl, B.; Ilbasimis-Tamer, S.; Degim, I.T.; Hunter, A.C.; Andresen, T.L.; Moghimi, S.M. Complement activation by PEG-functionalized multi-walled carbon nanotubes is independent of PEG molecular mass and surface density. *Nanomed. Nanotechnol. Biol. Med.* **2013**, *9*, 469–473. [[CrossRef](#)]
158. Burke, A.R.; Singh, R.N.; Carroll, D.L.; Owen, J.D.; Kock, N.D.; D'Agostino, R.; Torti, F.M.; Torti, S.V. Determinants of the thrombogenic potential of multiwalled carbon nanotubes. *Biomaterials* **2011**, *32*, 5970–5978. [[CrossRef](#)]
159. Sokolov, A.V.; Aseychev, A.V.; Kostevich, V.A.; Gusev, A.A.; Gusev, S.A.; Vlasova, I.I. Functionalization of single-walled carbon nanotubes regulates their effect on hemostasis. *J. Phys. Conf. Ser.* **2011**, *291*, 012054. [[CrossRef](#)]
160. Radomski, A.; Jurasz, P.; Alonso-Escolano, D.; Drews, M.; Morandi, M.; Malinski, T.; Radomski, M.W. Nanoparticle-induced platelet aggregation and vascular thrombosis. *Br. J. Pharmacol.* **2005**, *146*, 882–893. [[CrossRef](#)] [[PubMed](#)]
161. Nemmar, A.; Hoet, P.H.M.; Vandervoort, P.; Dinsdale, D.; Nemery, B.; Hoylaerts, M.F. Enhanced peripheral thrombogenicity after lung inflammation is mediated by platelet-leukocyte activation: Role of P-selectin. *J. Thromb. Haemost.* **2007**, *5*, 1217–1226. [[CrossRef](#)] [[PubMed](#)]
162. Bihari, P.; Holzer, M.; Praetner, M.; Fent, J.; Lerchenberger, M.; Reichel, C.A.; Rehberg, M.; Lakatos, S.; Krombach, F. Single-walled carbon nanotubes activate platelets and accelerate thrombus formation in the microcirculation. *Toxicology* **2010**, *269*, 148–154. [[CrossRef](#)]
163. Holzer, M.; Bihari, P.; Praetner, M.; Uhl, B.; Reichel, C.; Fent, J.; Vippola, M.; Lakatos, S.; Krombach, F. Carbon-based nanomaterials accelerate arteriolar thrombus formation in the murine microcirculation independently of their shape. *J. Appl. Toxicol.* **2014**, *34*, 1167–1176. [[CrossRef](#)]
164. Semberova, J.; De Paoli Lacerda, S.H.; Simakova, O.; Holada, K.; Gelderman, M.P.; Simak, J. Carbon nanotubes activate blood platelets by inducing extracellular Ca²⁺ influx sensitive to calcium entry inhibitors. *Nano Lett.* **2009**, *9*, 3312–3317. [[CrossRef](#)]
165. De Paoli Lacerda, S.H.; Semberova, J.; Holada, K.; Simakova, O.; Hudson, S.D.; Simak, J. Carbon nanotubes activate store-operated calcium entry in human blood platelets. *ACS Nano* **2011**, *5*, 5808–5813. [[CrossRef](#)]
166. Meng, J.; Cheng, X.; Liu, J.; Zhang, W.; Li, X.; Kong, H.; Xu, H. Effects of long and short carboxylated or aminated multiwalled carbon nanotubes on blood coagulation. *PLoS ONE* **2012**, *7*, 1–8. [[CrossRef](#)]
167. Fent, J.; Bihari, P.; Vippola, M.; Sarlin, E.; Lakatos, S. In vitro platelet activation, aggregation and platelet-granulocyte complex formation induced by surface modified single-walled carbon nanotubes. *Toxicol. Vitro.* **2015**, *29*, 1132–1139. [[CrossRef](#)]
168. Suk, J.S.; Xu, Q.; Kim, N.; Hanes, J.; Ensign, L.M. PEGylation as a strategy for improving nanoparticle-based drug and gene delivery. *Adv. Drug Deliv. Rev.* **2016**, *99*, 28–51. [[CrossRef](#)]
169. Vakhrusheva, T.V.; Gusev, A.A.; Gusev, S.A.; Vlasova, I.I. Albumin reduces thrombogenic potential of single-walled carbon nanotubes. *Toxicol. Lett.* **2013**, *221*, 137–145. [[CrossRef](#)]
170. Vlasova, I.I.; Mikhalchik, E.V.; Barinov, N.A.; Kostevich, V.A.; Smolina, N.V.; Klinov, D.V.; Sokolov, A.V. Adsorbed plasma proteins modulate the effects of single-walled carbon nanotubes on neutrophils in blood. *Nanomed. Nanotechnol. Biol. Med.* **2016**, *12*, 1615–1625. [[CrossRef](#)]
171. Canapè, C.; Foillard, S.; Bonafè, R.; Maiocchi, A.; Doris, E. Comparative assessment of the in vitro toxicity of some functionalized carbon nanotubes and fullerenes. *RSC Adv.* **2015**, *5*, 68446–68453. [[CrossRef](#)]

172. Donkor, A.D.; Su, Z.; Mandal, H.S.; Jin, X.; Tang, X.S. Carbon nanotubes inhibit the hemolytic activity of the pore-forming toxin pyolysin. *Nano Res.* **2009**, *2*, 517–525. [[CrossRef](#)]
173. Sachar, S.; Saxena, R.K. Cytotoxic effect of poly-dispersed single walled carbon nanotubes on erythrocytes in vitro and in vivo. *PLoS ONE* **2011**, *6*, 20–25. [[CrossRef](#)]
174. Bhardwaj, N.; Saxena, R.K. Selective loss of younger erythrocytes from blood circulation and changes in erythropoietic patterns in bone marrow and spleen in mouse anemia induced by poly-dispersed single-walled carbon nanotubes. *Nanotoxicology* **2015**, *9*, 1032–1040. [[CrossRef](#)]
175. Heo, Y.; Li, C.-A.; Kim, D.; Shin, S. Rheological alteration of erythrocytes exposed to carbon nanotubes. *Clin. Hemorheol. Microcirc.* **2017**, *65*, 49–56. [[CrossRef](#)]
176. Geim, A.K. Nobel Lecture: Random walk to graphene. *Rev. Mod. Phys.* **2011**, *83*, 851–862. [[CrossRef](#)]
177. Goenka, S.; Sant, V.; Sant, S. Graphene-based nanomaterials for drug delivery and tissue engineering. *J. Control. Release* **2014**, *173*, 75–88. [[CrossRef](#)]
178. Soldano, C.; Mahmood, A.; Dujardin, E. Production, properties and potential of graphene. *Carbon N. Y.* **2010**, *48*, 2127–2150. [[CrossRef](#)]
179. Vijayaraghavan, A. Graphene—Properties and characterization. In *Springer Handbook of Nanomaterials*; Springer: Berlin/Heidelberg, Germany, 2013; pp. 39–82, ISBN 9783642205958.
180. Sun, L. Structure and synthesis of graphene oxide. *Chin. J. Chem. Eng.* **2019**, *27*, 2251–2260. [[CrossRef](#)]
181. Paredes, J.I.; Villar-Rodil, S.; Martínez-Alonso, A.; Tascón, J.M.D. Graphene Oxide Dispersions in Organic Solvents. *Langmuir* **2008**, *24*, 10560–10564. [[CrossRef](#)] [[PubMed](#)]
182. Zhao, H.; Ding, R.; Zhao, X.; Li, Y.; Qu, L.; Pei, H.; Yildirimer, L.; Wu, Z.; Zhang, W. Graphene-based nanomaterials for drug and/or gene delivery, bioimaging, and tissue engineering. *Drug Discov. Today* **2017**, *22*, 1302–1317. [[CrossRef](#)] [[PubMed](#)]
183. Reina, G.; González-Domínguez, J.M.; Criado, A.; Vázquez, E.; Bianco, A.; Prato, M. Promises, facts and challenges for graphene in biomedical applications. *Chem. Soc. Rev.* **2017**, *46*, 4400–4416. [[CrossRef](#)]
184. Shim, G.; Kim, M.-G.; Park, J.Y.; Oh, Y.-K. Graphene-based nanosheets for delivery of chemotherapeutics and biological drugs. *Adv. Drug Deliv. Rev.* **2016**, *105*, 205–227. [[CrossRef](#)]
185. Jaleel, J.A.; Sruthi, S.; Pramod, K. Reinforcing nanomedicine using graphene family nanomaterials. *J. Control. Release* **2017**, *255*, 218–230. [[CrossRef](#)]
186. Zhang, Q.; Wu, Z.; Li, N.; Pu, Y.; Wang, B.; Zhang, T.; Tao, J. Advanced review of graphene-based nanomaterials in drug delivery systems: Synthesis, modification, toxicity and application. *Mater. Sci. Eng. C* **2017**, *77*, 1363–1375. [[CrossRef](#)]
187. Chen, Y.-W.; Su, Y.-L.; Hu, S.-H.; Chen, S.-Y. Functionalized graphene nanocomposites for enhancing photothermal therapy in tumor treatment. *Adv. Drug Deliv. Rev.* **2016**, *105*, 190–204. [[CrossRef](#)]
188. Gulzar, A.; Yang, P.; He, F.; Xu, J.; Yang, D.; Xu, L.; Jan, M.O. Bioapplications of graphene constructed functional nanomaterials. *Chem. Biol. Interact.* **2017**, *262*, 69–89. [[CrossRef](#)]
189. Zhu, X.; Liu, Y.; Li, P.; Nie, Z.; Li, J. Applications of graphene and its derivatives in intracellular biosensing and bioimaging. *Analyst* **2016**, *141*, 4541–4553. [[CrossRef](#)]
190. Peña-Bahamonde, J.; Nguyen, H.N.; Fanourakis, S.K.; Rodrigues, D.F. Recent advances in graphene-based biosensor technology with applications in life sciences. *J. Nanobiotechnol.* **2018**, *16*, 75. [[CrossRef](#)] [[PubMed](#)]
191. Wang, F.; Liu, L.; Li, W.J. Graphene-Based Glucose Sensors: A Brief Review. *IEEE Trans. Nanobiosci.* **2015**, *14*, 818–834. [[CrossRef](#)] [[PubMed](#)]
192. Zou, X.; Zhang, L.; Wang, Z.; Luo, Y. Mechanisms of the Antimicrobial Activities of Graphene Materials. *J. Am. Chem. Soc.* **2016**, *138*, 2064–2077. [[CrossRef](#)] [[PubMed](#)]
193. Wang, Q.; Li, Y.-H.; Jiang, W.-J.; Zhao, J.-G.; Xiao, B.-G.; Zhang, G.-X.; Ma, C.-G. Graphene-Based Nanomaterials: Potential Tools for Neurorepair. *Curr. Pharm. Des.* **2018**, *24*, 56–61. [[CrossRef](#)]
194. Shin, S.R.; Li, Y.C.; Jang, H.L.; Khoshakhlagh, P.; Akbari, M.; Nasajpour, A.; Zhang, Y.S.; Tamayol, A.; Khademhosseini, A. Graphene-based materials for tissue engineering. *Adv. Drug Deliv. Rev.* **2016**, *105*, 255–274. [[CrossRef](#)]
195. Zhang, Y.; Wu, C.; Zhang, J. Interactions of graphene and graphene oxide with proteins and peptides. *Nanotechnol. Rev.* **2013**, *2*, 27–45. [[CrossRef](#)]
196. Ding, Z.; Ma, H.; Chen, Y. Interaction of graphene oxide with human serum albumin and its mechanism. *RSC Adv.* **2014**, *4*, 55290–55295. [[CrossRef](#)]

197. Li, S.; Aphale, A.N.; MacWan, I.G.; Patra, P.K.; Gonzalez, W.G.; Miksovska, J.; Leblanc, R.M. Graphene oxide as a quencher for fluorescent assay of amino acids, peptides, and proteins. *ACS Appl. Mater. Interfaces* **2012**, *4*, 7069–7075. [[CrossRef](#)]
198. Wei, X.-Q.; Hao, L.-Y.; Shao, X.-R.; Zhang, Q.; Jia, X.-Q.; Zhang, Z.-R.; Lin, Y.-F.; Peng, Q. Insight into the Interaction of Graphene Oxide with Serum Proteins and the Impact of the Degree of Reduction and Concentration. *ACS Appl. Mater. Interfaces* **2015**, *7*, 13367–13374. [[CrossRef](#)]
199. Loh, K.P.; Lim, C.T. Molecular Hemocompatibility of Graphene Oxide and Its Implication for Antithrombotic Applications. *Small* **2015**, *11*, 5105–5117.
200. Chong, Y.; Ge, C.; Yang, Z.; Garate, J.A.; Gu, Z.; Weber, J.K.; Liu, J.; Zhou, R. Reduced Cytotoxicity of Graphene Nanosheets Mediated by Blood-Protein Coating. *ACS Nano* **2015**, *9*, 5713–5724. [[CrossRef](#)] [[PubMed](#)]
201. Feng, R.; Yu, Y.; Shen, C.; Jiao, Y.; Zhou, C. Impact of graphene oxide on the structure and function of important multiple blood components by a dose-dependent pattern. *J. Biomed. Mater. Res. Part A* **2015**, *103*, 2006–2014. [[CrossRef](#)] [[PubMed](#)]
202. Castagnola, V.; Zhao, W.; Boselli, L.; Lo Giudice, M.C.; Meder, F.; Polo, E.; Paton, K.R.; Backes, C.; Coleman, J.N.; Dawson, K.A. Biological recognition of graphene nanoflakes. *Nat. Commun.* **2018**, *9*, 1–9. [[CrossRef](#)] [[PubMed](#)]
203. Mao, H.; Chen, W.; Laurent, S.; Thirifays, C.; Burtea, C.; Rezaee, F.; Mahmoudi, M. Hard corona composition and cellular toxicities of the graphene sheets. *Colloids Surfaces B Biointerfaces* **2013**, *109*, 212–218. [[CrossRef](#)]
204. Qi, Y.; Chen, W.; Liu, F.; Liu, J.; Zhang, T.; Chen, W. Aggregation morphology is a key factor determining protein adsorption on graphene oxide and reduced graphene oxide nanomaterials. *Environ. Sci. Nano* **2019**, *6*, 1303–1309. [[CrossRef](#)]
205. Wibroe, P.P.; Petersen, S.V.; Bovet, N.; Laursen, B.W.; Moghimi, S.M. Soluble and immobilized graphene oxide activates complement system differently dependent on surface oxidation state. *Biomaterials* **2016**, *78*, 20–26. [[CrossRef](#)]
206. Belling, J.N.; Jackman, J.A.; Yorulmaz Avsar, S.; Park, J.H.; Wang, Y.; Potroz, M.G.; Ferhan, A.R.; Weiss, P.S.; Cho, N.-J. Stealth Immune Properties of Graphene Oxide Enabled by Surface-Bound Complement Factor H. *ACS Nano* **2016**, *10*, 10161–10172. [[CrossRef](#)]
207. Orecchioni, M.; Ménard-Moyon, C.; Delogu, L.G.; Bianco, A. Graphene and the immune system: Challenges and potentiality. *Adv. Drug Deliv. Rev.* **2016**, *105*, 163–175. [[CrossRef](#)]
208. Saleem, J.; Wang, L.; Chen, C. Immunological effects of graphene family nanomaterials. *NanoImpact* **2017**, *5*, 109–118. [[CrossRef](#)]
209. Mukherjee, S.P.; Bottini, M.; Fadeel, B. Graphene and the immune system: A romance of many dimensions. *Front. Immunol.* **2017**, *8*, 1–11. [[CrossRef](#)]
210. Sasidharan, A.; Panchakarla, L.S.; Sadanandan, A.R.; Ashokan, A.; Chandran, P.; Girish, C.M.; Menon, D.; Nair, S.V.; Rao, C.N.R.; Koyakutty, M. Hemocompatibility and Macrophage Response of Pristine and Functionalized Graphene. *Small* **2012**, *8*, 1251–1263. [[CrossRef](#)] [[PubMed](#)]
211. Singh, S.K.; Singh, M.K.; Nayak, M.K.; Kumari, S.; Shrivastava, S.; Grácio, J.J.A.; Dash, D. Thrombus Inducing Property of Atomically Thin Graphene Oxide Sheets. *ACS Nano* **2011**, *5*, 4987–4996. [[CrossRef](#)] [[PubMed](#)]
212. Zhang, X.; Yin, J.; Peng, C.; Hu, W.; Zhu, Z.; Li, W.; Fan, C.; Huang, Q. Distribution and biocompatibility studies of graphene oxide in mice after intravenous administration. *Carbon N. Y.* **2011**, *49*, 986–995. [[CrossRef](#)]
213. Liao, K.H.; Lin, Y.S.; MacOsco, C.W.; Haynes, C.L. Cytotoxicity of graphene oxide and graphene in human erythrocytes and skin fibroblasts. *ACS Appl. Mater. Interfaces* **2011**, *3*, 2607–2615. [[CrossRef](#)] [[PubMed](#)]
214. Monasterio, B.G.; Alonso, B.; Sot, J.; García-Arribas, A.B.; Gil-Cartón, D.; Valle, M.; Zurutuza, A.; Goñi, F.M. Coating Graphene Oxide with Lipid Bilayers Greatly Decreases Its Hemolytic Properties. *Langmuir* **2017**, *33*, 8181–8191. [[CrossRef](#)] [[PubMed](#)]
215. Ou, L.; Song, B.; Liang, H.; Liu, J.; Feng, X.; Deng, B.; Sun, T.; Shao, L. Toxicity of graphene-family nanoparticles: A general review of the origins and mechanisms. *Part. Fibre Toxicol.* **2016**, *13*, 57. [[CrossRef](#)]
216. Hu, X.; Li, D.; Mu, L. Biotransformation of graphene oxide nanosheets in blood plasma affects their interactions with cells. *Environ. Sci. Nano* **2017**, *4*, 1569–1578. [[CrossRef](#)]
217. Papi, M.; Lauriola, M.C.; Palmieri, V.; Ciasca, G.; Maulucci, G.; De Spirito, M. Plasma protein corona reduces the haemolytic activity of graphene oxide nano and micro flakes. *RSC Adv.* **2015**, *5*, 81638–81641. [[CrossRef](#)]

218. Wang, X.; Zhou, N.; Yuan, J.; Wang, W.; Tang, Y.; Lu, C.; Zhang, J.; Shen, J. Antibacterial and anticoagulation properties of carboxylated graphene oxide–lanthanum complexes. *J. Mater. Chem.* **2012**, *22*, 1673–1678. [[CrossRef](#)]
219. De Sousa, M.; Martins, C.H.Z.; Franqui, L.S.; Fonseca, L.C.; Delite, F.S.; Lanzoni, E.M.; Martinez, D.S.T.; Alves, O.L. Covalent functionalization of graphene oxide with d-mannose: Evaluating the hemolytic effect and protein corona formation. *J. Mater. Chem. B* **2018**, *6*, 2803–2812. [[CrossRef](#)]
220. Geng, H.; Wang, T.; Cao, H.; Zhu, H.; Di, Z.; Liu, X. Antibacterial ability, cytocompatibility and hemocompatibility of fluorinated graphene. *Colloids Surf. B Biointerfaces* **2019**, *173*, 681–688. [[CrossRef](#)] [[PubMed](#)]
221. Liu, X.; Cao, Y.; Zhao, M.; Deng, J.; Li, X.; Li, D. The enhanced anticoagulation for graphene induced by COOH⁺ ion implantation. *Nanoscale Res. Lett.* **2015**, *10*, 1–6. [[CrossRef](#)] [[PubMed](#)]
222. Kanakia, S.; Toussaint, J.D.; Mullick Chowdhury, S.; Tembulkar, T.; Lee, S.; Jiang, Y.P.; Lin, R.Z.; Shroyer, K.R.; Moore, W.; Sitharaman, B. Dose ranging, expanded acute toxicity and safety pharmacology studies for intravenously administered functionalized graphene nanoparticle formulations. *Biomaterials* **2014**, *35*, 7022–7031. [[CrossRef](#)] [[PubMed](#)]
223. Zare-Zardini, H.; Taheri-Kafrani, A.; Ordooei, M.; Amiri, A.; Karimi-Zarchi, M. Evaluation of toxicity of functionalized graphene oxide with ginsenoside Rh2, lysine and arginine on blood cancer cells (K562), red blood cells, blood coagulation and cardiovascular tissue: In vitro and in vivo studies. *J. Taiwan Inst. Chem. Eng.* **2018**, *93*, 70–78. [[CrossRef](#)]
224. Geldert, A.; Liu, Y.; Loh, K.P.; Lim, C.T. Nano-bio interactions between carbon nanomaterials and blood plasma proteins: Why oxygen functionality matters. *NPG Asia Mater.* **2017**, *9*, e422.
225. Mesarič, T.; Baweja, L.; Drašler, B.; Drobne, D.; Makovec, D.; Dušak, P.; Dhawan, A.; Sepčić, K. Effects of surface curvature and surface characteristics of carbon-based nanomaterials on the adsorption and activity of acetylcholinesterase. *Carbon N. Y.* **2013**, *62*, 222–232. [[CrossRef](#)]
226. Mu, Q.; Liu, W.; Xing, Y.; Zhou, H.; Li, Z.; Zhang, Y.; Ji, L.; Wang, F.; Si, Z.; Zhang, B.; et al. Protein binding by functionalized multiwalled carbon nanotubes is governed by the surface chemistry of both parties and the nanotube diameter. *J. Phys. Chem. C* **2008**, *112*, 3300–3307. [[CrossRef](#)]
227. Wang, X.; Zhu, Y.; Chen, M.; Yan, M.; Zeng, G.; Huang, D. How do proteins ‘response’ to common carbon nanomaterials? *Adv. Colloid Interface Sci.* **2019**, *270*, 101–107. [[CrossRef](#)]
228. Belime, A.; Thielens, N.M.; Gravel, E.; Frachet, P.; Ancelet, S.; Tacnet, P.; Caneiro, C.; Chuprin, J.; Gaboriaud, C.; Schoehn, G.; et al. Recognition protein C1q of innate immunity agglutinates nanodiamonds without activating complement. *Nanomed. Nanotechnol. Biol. Med.* **2019**, *18*, 292–302. [[CrossRef](#)]



© 2020 by the author. Licensee MDPI, Basel, Switzerland. This article is an open access article distributed under the terms and conditions of the Creative Commons Attribution (CC BY) license (<http://creativecommons.org/licenses/by/4.0/>).